Antiviral Research 219 (2023) 105734

Contents lists available at ScienceDirect

Antiviral Research

journal homepage: www.elsevier.com/locate/antiviral

Mechanisms of antiviral activity of the new *h*DHODH inhibitor MEDS433 against respiratory syncytial virus replication

Anna Luganini [a,1], Giulia Sibille [a,1], Marta Pavan [a], Maurizia Mello Grand [c], Stefano Sainas [b], Donatella Boschi [b], Marco L. Lolli [b], Giovanna Chiorino [c], Giorgio Gribaudo [a,*]

[a] *Department of Life Sciences and Systems Biology, University of Torino, 10123, Torino, Italy*
[b] *Department of Drug Sciences and Technology, University of Torino, 10125, Torino, Italy*
[c] *Fondazione Edo ed Elvo Tempia, 13900, Biella, Italy*

ARTICLE INFO

Keywords:
Respiratory syncytial virus
Pyrimidine biosynthesis
*h*DHODH
MEDS433
ISG proteins
Human small airway epithelium

ABSTRACT

Human respiratory syncytial virus (RSV) is an important cause of acute lower respiratory infections, for which no effective drugs are currently available. The development of new effective anti-RSV agents is therefore an urgent priority, and Host-Targeting Antivirals (HTAs) can be considered to target RSV infections. As a contribution to this antiviral avenue, we have characterized the molecular mechanisms of the anti-RSV activity of MEDS433, a new inhibitor of human dihydroorotate dehydrogenase (*h*DHODH), a key cellular enzyme of *de novo* pyrimidine biosynthesis. MEDS433 was found to exert a potent antiviral activity against RSV-A and RSV-B in the one-digit nanomolar range. Analysis of the RSV replication cycle in MEDS433-treated cells, revealed that the *h*DHODH inhibitor suppressed the synthesis of viral genome, consistently with its ability to specifically target *h*DHODH enzymatic activity. Then, the capability of MEDS433 to induce the expression of antiviral proteins encoded by Interferon-Stimulated Genes (ISGs) was identified as a second mechanism of its antiviral activity against RSV. Indeed, MEDS433 stimulated secretion of IFN-β and IFN-λ1 that, in turn, induced the expression of some ISG antiviral proteins, such as IFI6, IFITM1 and IRF7. Singly expression of these ISG proteins reduced RSV-A replication, thus likely contributing to the overall anti-RSV activity of MEDS433. Lastly, MEDS433 proved to be effective against RSV-A replication even in a primary human small airway epithelial cell model. Taken as a whole, these observations provide new insights for further development of MEDS433, as a promising candidate to develop new strategies for treatment of RSV infections.

1. Introduction

The Respiratory syncytial virus (RSV) is a leading cause of lower respiratory tract infections (LRTI) that may give rise to severe illnesses, such as bronchiolitis and pneumonia in high-risk groups, including children, adults with a compromised immune system or with comorbidities, and elderly (Jorquera et al., 2016; Jain et al., 2022). Globally, in children aged 0–60 months, RSV infections cause more than 33 million LRTI per year, that lead to an estimated 3.6 million hospitalizations, and around 100,000 in-hospital deaths (Li et al., 2022). RSV infections, however, constitute a substantial disease burden even in adults aged ≥65 years (Nam and Ison, 2019). In fact, it is estimated that 160,000 older adults are hospitalized, and 10,000 of them die due to RSV infection (Hansen et al., 2022). Hence, RSV is a contagious seasonal virus causing significant morbidity and mortality both in pediatric and adult settings.

These days, prevention of RSV infections in adults can be achieved by means of two new RSV prefusion F protein-based vaccines approved in 2023, such as Abrysvo (Pfizer) and Arexvy (GSK) (Soni et al., 2023). However, no RSV vaccine is available yet for infants and young children, for whom the only useable prophylaxis is still based on neutralizing mAbs directed against the F glycoprotein, such as Palivizumab (Garegnani et al., 2021), and the recently approved Nirsevimab (Hammitt et al., 2022; Simões et al., 2023). In contrast, options for treatment of RSV infections are limited to supportive care with bronchodilators and supplemental oxygen (Broadbent et al., 2015), since the only approved antiviral drug against RSV, ribavirin (RBV), is exclusively restricted to hospitalized infants and young children with severe LRTIs (Jain et al., 2022; Tejada et al., 2022). However, concerns about RBV safety and

* Corresponding author. Department of Life Sciences and Systems Biology, University of Torino, Via Accademia Albertina 13, 10123, Torino, Italy.
E-mail address: giorgio.gribaudo@unito.it (G. Gribaudo).
[1] Co-first author: A.L. and G.S. contributed equally to this work.

https://doi.org/10.1016/j.antiviral.2023.105734
Received 25 July 2023; Received in revised form 14 October 2023; Accepted 15 October 2023
Available online 16 October 2023

Abbreviations

HTA	Host-targeting antivirals
DHODH	Dihydroorotate dehydrogenase
ISGs	Interferon Stimulated Genes
RBV	Ribavirin
BSA	Broad-spectrum antivirals
VRA	Virus yield reduction assay
TOA	Time-of-addition
Fa	Fractional effect analysis

efficacy, discourage its clinical use (Beaird et al., 2016). Therefore, given the public health impact of RSV infections on a global scale, as well as the paucity of the current anti-RSV intervention arsenal, the development of new effective antiviral agents to mitigate or reduce the disease burden is an urgent priority.

To meet this need, host-targeting antiviral (HTAs) interfering with cellular biochemical pathways essential for RSV replication may be taken into consideration, as believable alternatives to the *de novo* development of direct-acting antivirals (DAA) targeting specific RSV proteins. In fact, HTAs prevent viral drug resistance and are amenable to be developed as broad-spectrum antivirals (BSA) effective against different viruses (Heylen et al., 2017; Amarelle and Lecuona, 2018).

Considering that the availability of appropriate pyrimidine pools in infected cells is mandatory for efficient viral replication, pharmacological targeting of the pyrimidine biosynthesis pathway is thus a plausible strategy to develop effective HTAs (Okesli et al., 2017; Löffler et al., 2020). Especially, in virus-infected cells, such as those infected with RSV, in which the *de novo* pyrimidine biosynthesis pathway is activated during viral infection to meet the high pyrimidine demand tied to viral gene expression and replication (Gribaudo et al., 2002, 2003; Munger et al., 2008; Martín-Vicente et al., 2020; Karimi et al., 2022). In this regard, the activity of the human dihydroorotate dehydrogenase (*h*DHODH), a mitochondrial enzyme that catalyzes the oxidation of dihydroorotic acid (DHO) to orotic acid (ORO), as a critical step in the biosynthesis of uridine and cytidine (Reis et al., 2017; Löffler et al., 2020), may represent a druggable target of choice to interfere with the replication of RNA viruses (Okesli et al., 2017; Boschi et al., 2019; Coelho and Oliveira, 2020).

To contribute to this intervention avenue, we designed and characterized a small molecule *h*DHODH inhibitor, MEDS433, that is being developed in the perspective of a new HTA. MEDS433 is in fact a potent inhibitor of *h*DHODH (IC_{50} 1.2 nM) that interacts with the enzyme's ubiquinone binding site (Sainas et al., 2018, 2021, 2022). Recently, we have observed that MEDS433 inhibits the *in vitro* replication of herpes simplex virus type 1 (HSV-1) and type 2 (HSV-2) (Luganini et al., 2021), influenza A and B viruses (Sibille et al., 2022), as well as of different human coronaviruses (CoVs), such as the α-hCoV-229E and the β-CoVs hCoV-OC43 and SARS-CoV-2 (Calistri et al., 2021), in the nanomolar range.

Based on these facts, this study intended to expand the potential of MEDS433 as a BSA against respiratory viruses by investigating its activity against RSV. Here, we report on the characterization of the mechanisms by which MEDS433 impairs RSV replication. Especially, MEDS433 was observed to bring about both a direct inhibition of viral RNA genome synthesis, and the induction of antiviral proteins encoded by interferon-stimulated genes (ISG) able to hamper RSV replication. These results confirm once more MEDS433 as a promising HTA and suggest its suitability to design new intervention strategies for RSV infections.

2. Materials and methods

2.1. Compounds

MEDS433 and brequinar were synthesized as previously described (Madak et al., 2017; Sainas et al., 2018). Ribavirin (RBV), uridine (UR), cytidine (CT), orotic acid (OA), dihydroorotic acid (DHO), dipyridamole (DPY), teriflunomide, and human recombinant interferon-alpha-1 (IFN-α) were purchased from Merck. ASLAN003 was obtained from MedChem Express. All compounds were resuspended in 100% DMSO, except IFN-α, which was resuspended in sterile water.

2.2. Cells and viruses

The human adenocarcinoma alveolar basal epithelial A549 (ATCC CCL-185) and the human laryngeal squamous carcinoma HEp-2 (ATCC CCL-23) cell lines were purchased from the American Type Culture Collection (ATCC), the Lenti-X 293T cell line was obtained from Takara. Cells were cultured in Dulbecco's Modified Eagle Medium (DMEM; Euroclone) supplemented with 10% fetal bovine serum (FBS, Euroclone), 2 mM glutamine, 1 mM sodium pyruvate, 100 U/ml penicillin, and 100 μg/ml streptomycin sulfate (Euroclone).

Primary 3D human small airway epithelial tissues (SmallAir™) were obtained from Epithelix, (EP21) and were isolated from the bronchiolar region of healthy donors and cultured on transwell inserts at air-liquid interface (ALI), as ready-formed pseudostratified epithelial layers. ALI cultures were maintained until use according to the manufacturer's protocol.

RSV strain Long A (ATCC VR-26) and RSV strain B (ATCC VR-955) were propagated in HEp-2 cells by infecting 90% confluent monolayers at a virus-to-cell ratio (MOI) of 0.01 and cultured in DMEM supplemented with 2% FBS. Viral stocks were prepared after three rounds of cell freezing and thawing, and centrifugal clarification. Supernatants were then added to equal volumes of 50% sucrose for stabilization. Virus titers were measured by standard plaque assays on HEp-2 cells.

2.3. Antiviral assays

The anti-RSV activity of MEDS433, brequinar, or RBV was measured by the plaque reduction assay (PRA) in HEp-2 cells or by the virus yield reduction assay (VRA) in A549 cells. For PRA, HEp-2 cells (120,000 cells/well) were seeded in 48-well plates, and after 24 h, treated 1 h prior to infection with different compounds concentrations, and then infected with RSV-A or RSV-B (30 PFU/well) in the presence of compounds. After virus adsorption (2 h at 37 °C), viral inocula were removed, and cells incubated in medium containing the corresponding compounds, 0.3% methylcellulose (Sigma-Aldrich) and 2% FBS. At 72 h post-infection (p.i.), cell monolayers were fixed, and stained with crystal violet. Viral plaques were then microscopically counted, and the mean plaque counts for each drug concentration was converted in viral titer (PFU/ml). The GraphPad Prism software version 8.0 was used to determine the concentration of compounds that produced 50 and 90% reductions in plaque formation (EC_{50} and EC_{90}).

For the VRA, A549 cells (120,000 cells/well) seeded in 48-well plates were treated with increasing concentrations of compounds, and then infected with RSV-A or RSV-B at an MOI of 0.01 PFU/cell. After virus adsorption, cells were incubated in medium containing the corresponding compounds. At 72 h p.i., the cell supernatants were harvested, and the RSV yield titrated by plaque assay on HEp-2 cells.

To evaluate the effect of UR, CT, ORO, or DHO addition, PRAs were performed with HEp-2 cells infected with RSV-A, and treated with increasing concentrations of UR, CT, ORO or DHO in presence of 0.05 μM of MEDS433. Compounds were maintained throughout the assay, and at 72 h p.i., cell monolayers were fixed, stained with crystal violet, and viral plaques microscopically counted.

To investigate the effect of blocking both the *de novo* biosynthesis and the salvage pathway of pyrimidines, in the absence or presence of UR, PRAs were performed in HEp-2 cells infected with RSV-A, and exposed throughout the assay to different concentration of MEDS433 in combination with increasing concentrations of DPY (1, 3, 5 μM) in medium supplemented with a hyper-physiological concentration of uridine (20 μM). At 72 h p.i., cell monolayers were fixed, stained and viral plaques microscopically counted.

For time-of-addition (TOA) studies, HEp-2 cells were seeded at a density of 240,000 cells/well in 24-well plates. The following day, cells monolayers were treated with 0.05 μM MEDS433 from −3 to −2 h prior to infection before infection with RSV-A (MOI of 0.1 PFU/cell) (pre-treatment, PRE-T); or during infection (adsorption stage, from −2 to 0 h, co-treatment, CO-T); or after virus adsorption (from 0 to 48 h p.i., post-treatment, POST-T); or throughout the experiment (full treatment, Full-T). At 48 h p.i., cell supernatants were harvested, and titrated for RSV-A infectivity on HEp-2 cells as described above.

The effects of two- (MEDS433 and RBV), or three-drug combination (MEDS433, RBV, and DPY) were assessed by PRAs as described above. MEDS433 and RBV, alone or in combination, were added on HEp-2 cell monolayers at equipotent ratio of at 0.25 × , 0.5 × , 1 × , 2 × , and 4 × EC_{50} of each drug. For the three-drug combination, DPY (3 μM) was added to the MEDS433 and RBV concentrations used in the two-drug combination. The effect of the two- or three-drug combination was then assessed by the Chou-Talalay method (Chou, 2006), based on the median-effect principle of the mass-action law computed in the CompuSyn software (Chou and Martin, 2005) (http://www.combosyn.com). With the Chou-Talalay method, a Combination Index (CI) = 1 represents an additive effect, a CI value > 1 means antagonism, and a CI value < 1 indicates synergism.

Primary small air epithelial cultures were treated basally 1 h before infection with 1, 5, or 10 μM MEDS433. Afterwards, epithelia cultures were infected apically with RSV-A at an MOI of 0.02 PFU/cell (input, time = 0 h), and incubated at 37 °C for 3 h in presence of compound. Viral inocula were then removed, and epithelia cultures washed twice with culture medium, then 200 μl of medium was added apically for 20 min to collect any residual viral particle (time = 3 h). Basal medium containing MEDS433 was changed daily, and apical washes were performed as above to harvest RSV virus particles release at 24, 48, 72, and 96 h p.i. time-points. Supernatants were then titrated for RSV infectivity on HEp-2 cell monolayers as described above, while epithelium cultures were formalin-fixed at 96 h p.i., paraffin-embedded, sectioned at a thickness of 4 μm, and stained with hematoxylin-eosin for microscopic analysis.

2.4. Cytotoxicity assay

Cytotoxicity was evaluated at 72 h post-treatment on A549 or HEp-2 cells using the CellTiter-Glo assay (Promega). To determine the cytotoxic effect of MEDS433 on primary small air epithelial cells, at each time-point the basal medium was harvested, and the LDH-Glo Cytotoxicity Assay (Promega) was performed following the manufacturer's instructions.

2.5. Quantitative real time PCR

HEp-2 cells were seeded in a 6-well plate (600,000 cells/well) and, after 24 h, treated with 0.05 μM MEDS433 1h prior to and during infection with RSV-A at an MOI of 0.1 PFU/cell. At different times p.i., cells were harvested, and RNA was extracted and purified by using an RNA purification kit (Macherey-Nagel). The levels of RSV-A RNA were then assessed by quantitative real time PCR using a GENESIG standard kit (Primerdesign). RSV genomic copy numbers were expressed as the normalized RNA copy number per nanogram of total RNA.

2.6. Gene expression profiling

Cultures of HEp-2 cells seeded in 6-well plates (1,000,000 cells/well) were left untreated or exposed to 1 μM of MEDS433 for 16 h. Thereafter, a culture of both untreated or MEDS433-treated cell monolayers was infected with RSV-A at an MOI of 1 PFU/cell. For the MEDS433-treated and RSV-infected cells, the compound was maintained during viral infection. At 24 h p.i., all cell samples were harvested, and total RNA was isolated by means of miRNeasy Mini kit (Qiagen). TURBO DNA Free kit (Thermo Fisher Scientific) was used to remove contaminating DNA. RNA quality and quantity were assessed using Agilent 2100 bioanalyzer (Agilent Technologies) and NanoDrop ND-1000 Spectro-photometer (Thermo Fisher Scientific), respectively. Gene expression profiling was carried out using the Agilent one-color labelling method. Labeling, hybridization, washing, and slide scanning were performed following the manufacturer's protocols. Briefly, mRNA from 100 ng of tot RNA was amplified, labeled with Cy3 and purified. Six-hundred ng of labeled specimens were then hybridized on Agilent Human Gene Expression v3 8 × 60K microarrays. After 17 h of hybridization, slides were washed and scanned using the Agilent Scanner (G2505C, Agilent Technologies).

Images were analyzed using the Feature Extraction software version 10.7.3.1 (Agilent Technologies). Raw data elaboration was carried out with Bioconductor (www.bioconductor.org), using LIMMA (LInear Models for Microarray Analysis) R package. Background correction was performed with the *normexp* method with an offset of 50, and *quantile* was used for the between-array normalization. The empirical Bayes method was used to compute a moderated t-statistics for two-class comparisons. MeV version 4.9.0 was used for unsupervised hierarchical clustering, and heatmap generation was performed on selected groups of genes and experimental conditions.

2.7. hDHODH gene knockdown

For RNA interference, A549 cells were transfected with a universal scrambled negative control siRNA (SR30004, Origene), or a *h*DHODH-targeting small interfering RNA (siRNA) (SR319917C, Origene) using the siTran 2.0 siRNA Transfection Reagent (TT320002, Origene). The content of the *h*DHODH protein was then measured at 72 h post-transfection by immunoblotting with a mouse anti-*h*DHODH mAb (SC-166348, Santa Cruz Biotechnology). To assess the effect of the *h*DHODH knockdown on RSV-A replication, at 24 h post-transfection, A549 cells were infected with RSV-A at an MOI of 0.01 PFU/cell, and after 72 h p.i., cell supernatants were harvested, and titrated on HEp-2 cells.

2.8. Analysis of proteins

For immunoblotting, HEp-2 cell monolayers were left untreated or treated with 1 μM of MEDS433, or with 100 ng/ml of IFNα for 24 or 48 h. Protein extracts were then prepared as previously described (Luganini et al., 2008), and equal amounts were fractionated by 4–15% SDS-PAGE and then transferred to PVDF membranes (BioRad). Filters were blocked for 2 h at 37 °C in EveryBlot Blocking Buffer (BioRad), and immunostained with either the mouse anti-*h*DHODH mAb (E−8, Santa Cruz Biotechnology), or the rabbit anti-IFI6 pAb (54355, Cell Signaling Technology, CST), or the rabbit anti-IFITM1 pAb (13126, CST), or the rabbit anti-IRF-7 mAb (D2A1J, CST), or the rabbit anti-IRF-1 mAb (D5E4, CST), or the rabbit anti-OAS2 pAb (54155, CST), or the rabbit anti-IRF3 mAb (D6I4C, CST), or the rabbit anti-phospho IRF3 (Ser 386) (E7J8G, CST). A rabbit anti-vinculin mAb (E1E9V, CST) or a rabbit anti-GAPDH mAb (D16H11, CST) were used as controls for protein loading. Immunocomplexes were then detected with goat anti-mouse Ig Ab or goat anti-rabbit Ig Ab conjugated to horseradish peroxidase (Life Technologies) and visualized by enhanced chemiluminescence (Clarity Western ECL Substrate, BioRad).

IFN-α IFN-β, IFN-λ1, or IFN-λ2 were quantified in cell supernatants using VeriKine-HS Human IFN-α All Subtype and IFN-β TCM ELISA Kits

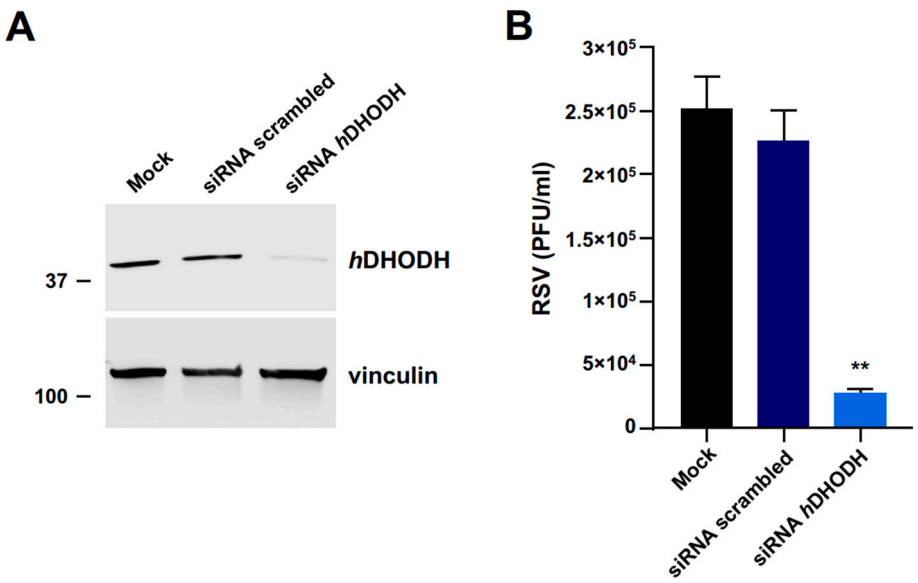

Fig. 1. Knockdown of *h*DHODH affects RSV replication. (**A**) *h*DHODH protein content in A549 cells mock-transfected or transfected with a scrambled negative control or *h*DHODH siRNAs. At 72 h after transfection, total protein extracts were analyzed by immunoblotting with an anti-*h*DHODH mAb. Immunodetection of vinculin was used as a control for protein loading. Molecular weight markers are indicated at the left side of each panel. (**B**) RSV yield from A549 cells mock-transfected or transfected with scrambled or *h*DHODH siRNAs. At 24 h after transfection, cells were infected with RSV-A at an MOI of 0.01 PFU/cell, and after 72 h p.i., cell supernatants were recovered, and titrated by plaque assay in HEp-2 cells. Data shown are the means ± SD (error bars) of $n = 2$ independent experiments performed in triplicate and analyzed by Kruskal-Wallis Dunn's multiple comparison test compared to the calibrator sample (Mock). **, $p < 0.005$.

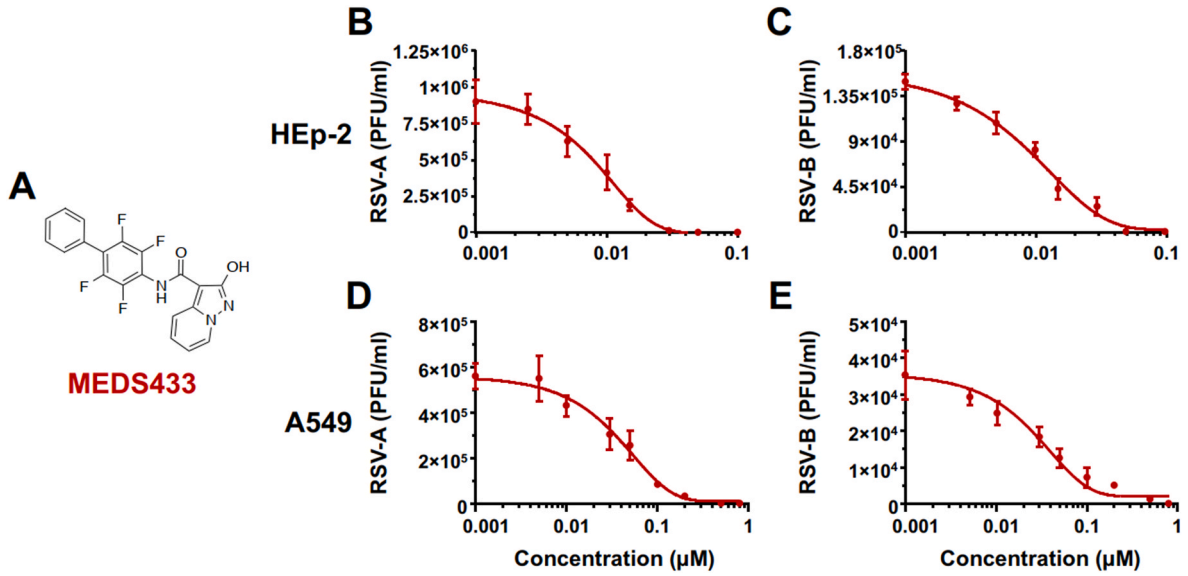

Fig. 2. MEDS433 inhibits the replication of RSV-A and RSV-B. (**A**) Chemical structure of MEDS433. (**B**, **C**) PRAs were performed in HEp-2 cells infected with RSV-A (**B**) or RSV-B (**C**) and treated with increasing concentrations of MEDS433 1 h before, during, and post-infection. At 72 h p.i., the viral plaques were microscopically counted and converted in viral titer (PFU/ml). (**D**, **E**) VRAs were performed in A549 cell monolayers infected with RSV-A (**D**) or RSV-B (**E**) and treated with increasing concentrations of MEDS433 throughout the experiment. At 72 h p.i., cell supernatants were harvested, and titrated by the plaque assay in HEp-2 cells. Data shown are the means ± SD of $n = 3$ independent experiments performed in triplicate.

(PBL Assay Science), or Human IFN-λ1 and IFN-λ2 ELISA kits (Innovative Research, Inc.), according to the manufacturers' instructions.

To neutralize IFN-β and IFN-λ1 in cell supernatants, murine neutralizing mAbs against IFN-β and IFN-λ1 (InvivoGen) were added to untreated or MEDS433-treated HEp-2 cell cultures at a concentration of 10 μg/ml.

2.9. Lentiviral vectors

Human IFI6, IFITM1, and IRF7 cDNAs purchased from Origene (SC112388, SC117830 and SC126916, respectively) were cloned into the pLVX-TetOne vector (Takara). Lentiviral vectors (LV) for doxycycline-inducible expression of IFI6, IFITM1 and IRF-7 proteins were generated in Lenti-X 293T cells by transfection of pLVX-TetOne containing IFI6, IFITM1, or IRF7 cDNAs, and the Lenti-X™ Tet-One™ Inducible Expression System (Takara) according to the manufacturer's instructions. At 48 h after transfection, LV-containing supernatants were collected and titrated using the Lenti-X™ qRT-PCR Titration kit (Takara). LV-transduced HEp-2 cell lines were then generated by infecting HEp-2 cell monolayers with LV-empty, or LV-IFI6, or LV-

Table 1
Antiviral activity of *h*DHODH inhibitors and ribavirin against RSV strains.

Compound	Cell line	RSV	EC_{50} (μM)[a]	EC_{90} (μM)[b]	CC_{50} (μM)[c]	SI[d]
MEDS433	HEp-2	RSV-A	0.0078 ± 0.00006	0.020 ± 0.00009	84.30 ± 0.574	10808
		RSV-B	0.0083 ± 0.00004	0.025 ± 0.00021		10157
	A549	RSV-A	0.0381 ± 0.00022	0.136 ± 0.00089	64.25 ± 3.125	1686
		RSV-B	0.0277 ± 0.00018	0.120 ± 0.00102		2319
Brequinar	HEp-2	RSV-A	0.0113 ± 0.00005	0.0311 ± 0.00016	71.70 ± 0.341	6345
		RSV-B	0.0190 ± 0.00012	0.0322 ± 0.00021		3774
Teriflunomide	HEp-2	RSV-A	8.58 ± 0.309	21.91 ± 0.187	109.22 ± 0.742	13
		RSV-B	6.54 ± 0.278	18.94 ± 0.611		17
ASLAN003	HEp-2	RSV-A	0.59 ± 0.088	2.41 ± 0.204	>400	>678
		RSV-B	0.64 ± 0.029	2.47 ± 0.125		>625
Ribavirin	HEp-2	RSV-A	2.3760 ± 0.0117	>10	240.46 ± 5.691	101
		RSV-B	1.3264 ± 0.0105	6.0315 ± 0.03949		181

[a] EC_{50}, compound concentration that inhibits 50% of virus replication, as determined against RSV-A and RSV-B by PRAs in HEp-2 cells, and by VRAs in A549 cells.
[b] EC_{90}, compound concentration that inhibits 90% of RSV-A or RSV-B replication, as determined by PRAs in HEp-2 cells, and by VRAs in A549 cells.
[c] CC_{50}, compound concentration that produces 50% of cytotoxicity, as determined by cell viability assays in HEp-2 and A549 cells. Reported values represent the means ± SD of data derived from three experiments in triplicate.
[d] SI, selectivity index determined as the ratio between CC_{50} and EC_{50}.

IFITM1, or LV-IRF7, at an MOI of 1, in the presence of 4 μg/ml of polybrene. Stable LV-transduced HEp-2-derived cell lines were obtained by selection in medium containing 2.5 μg/ml puromycin. The inducible expression of IFI6, IFITM1, or IRF7 proteins was achieved by stimulating the corresponding LV-derived cell line with doxycycline (100 ng/ml).

2.10. Statistical analysis

All statistical tests were performed using GraphPad Prism version 8.0 (GraphPad Software). Antiviral assays data are presented as the means ± SD of at least three experiments performed in triplicate. P values ≤ 0.05 were considered significant.

3. Results

3.1. Efficient RSV replication needs hDHODH expression

To appreciate the relevance of *h*DHODH for the completion of RSV productive replication, its expression was knocked down by means of siRNAs in the relevant cell model of human alveolar basal epithelial cells A549 (Fig. 1A). In comparison with mock-transfected A549 cells or cells transfected with a scrambled negative siRNA, the reduced level of *h*DHODH protein content significantly affected RSV-A replication with about 10-fold reduction of released infectious virus at 72 h post infection (h p.i.) (Fig. 1B). This observation thus indicated that optimal RSV replication necessitates *h*DHODH expression.

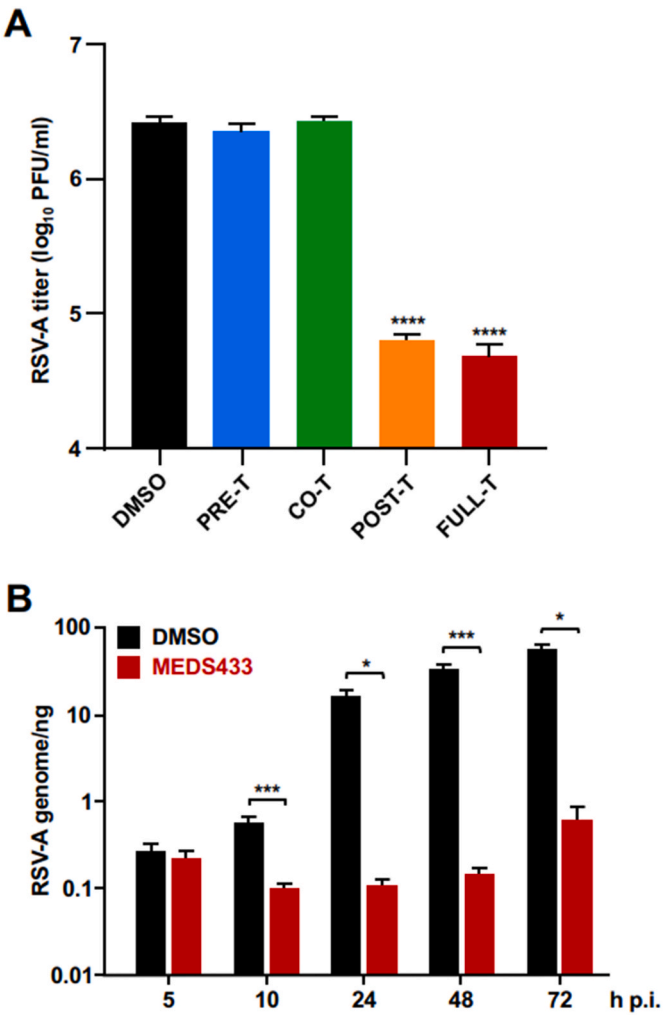

Fig. 3. MEDS433 abolishes RSV genome synthesis. (**A**) MEDS433 acts a post-entry stage of the RSV replication cycle. HEp-2 cells monolayers were infected with RSV-A at an MOI of 0.1 and where indicated, treated with 0.05 μM MEDS433 prior to infection (from −3 to −2 h prior, PRE-T), or during the infection (from −2 to 0 h p.i., CO-T); or after virus infection (from 0 to 48 h p.i., POST-T); or from −3 to 48 h p.i. (FULL-T). Control RSV-A-infected cells were exposed to vehicle DMSO only. At 48 h p.i., infectious RSV particles released in cell supernatants were titrated by plaque assay in HEp-2 cells. The data shown are the mean ± SD of $n = 2$ independent experiments performed in triplicate and analyzed by a one-way ANOVA followed by Dunnett's multiple comparison test. ****, $p < 0.0001$ compared to the calibrator sample (DMSO). (**B**) MEDS433 inhibits RSV RNA replication. HEp-2 cell monolayers were infected with RSV-A at an MOI of 0.1, and, where indicated, the infected cells were exposed to 0.05 μM MEDS433 or 0.02% DMSO. At 5, 10, 24, 48, and 72 h p.i., total RNA was isolated, and qPCR performed with appropriate RSV-A primers and probe. RSV-A RNA genomic copies were normalized per nanogram of RNA. The data shown are the means ± SD of $n = 2$ independent experiments performed in triplicate and analyzed by unpaired *t*-test compared to the calibrator sample (DMSO). *, $p < 0.05$; ***, $p < 0.001$.

3.2. The hDHODH inhibitor MEDS433 restricts RSV replication

Seeing that *h*DHODH expression is required for RSV replication, the pharmacological targeting of its enzymatic activity may represent a strategy to develop new anti-RSV agents. To this end, the anti-RSV activity of the new *h*DHODH inhibitor MEDS433 (Fig. 2A) was investigated by plaque reduction assay (PRA) in HEp-2 cells infected with RSV-A or RSV-B. Fig. 2 (panels B and C) shows that MEDS433 inhibited RSV-A and RSV-B plaque formation in a dose-dependent manner. The EC_{50} and EC_{90} were 0.0078 ± 0.00006 μM and 0.020 ± 0.00009 μM for RSV-

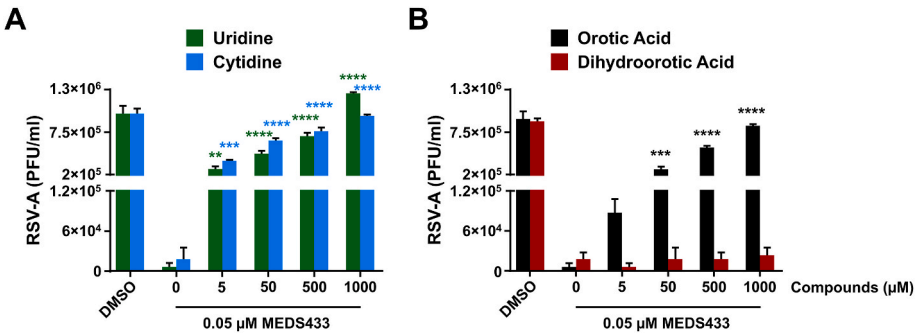

Fig. 4. The anti-RSV activity of MEDS433 is reversed by uridine, cytidine and orotic acid. HEp-2 cell monolayers were exposed to 0.05 μM of MEDS433 in the presence or absence of increasing concentrations of uridine and cytidine (**A**), dihydroorotic acid and orotic acid (**B**) before and during infection with RSV-A (30 PFU/well). Following virus adsorption, cells were incubated in the presence of compounds and, at 72 h.p.i., viral plaques were stained, microscopically counted, and plotted as PFU/ml. Control RSV-A-infected cells were exposed to vehicle DMSO only (DMSO). The data shown represent means ± SDs of $n = 3$ independent experiments performed in triplicate and analyzed by a two-way ANOVA, followed by Dunnett's multiple comparison test, versus to the calibrator sample (MEDS433 alone). **, $p < 0.005$; ***, $p < 0.001$; ****, $p < 0.0001$.

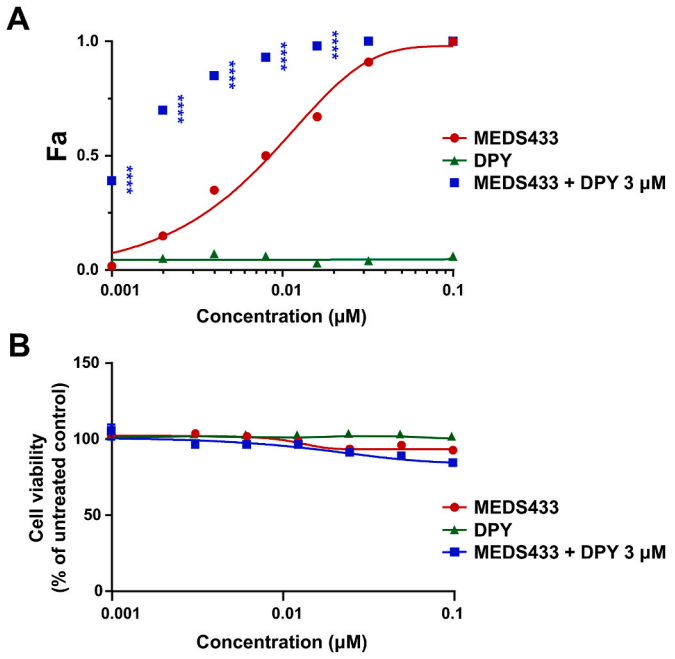

Fig. 5. The combination of MEDS433 and DPY is synergistic against RSV replication. (**A**) PRAs were performed in HEp-2 cells exposed to different concentrations of MEDS433 alone, or in combination with different amounts of DPY. At 72 h after RSV-A infection (30 PFU/well), viral plaques were stained, and microscopically counted. The effect of the combination was then analyzed by the CompuSyn software and displayed as a fractional effect analysis (Fa) plot in relation to the compound concentrations. The antiviral activity of MEDS433 and DPY, when used as single agents is depicted by red and green Fa curves, respectively. The effect of the MEDS433-DPY combination is shown with blue squares. Results are representative of $n = 3$ independent experiments performed in triplicate and analyzed by a two-way ANOVA, followed by Sidak's multiple comparison test. Statistical analysis was performed by comparing MEDS433-treated samples with the MEDS433 + DPY-treated samples for each condition. **** ($p < 0.0001$). (**B**) To determine cell viability, HEp-2 cell monolayers were exposed to different concentrations of MEDS433 alone or in combination with different amounts of DPY, or vehicle (DMSO) as control. After 72 h of incubation, the number of viable cells was determined by the CellTiter-Glo Luminescent assay. Results are shown as means ± SD (error bars) of three independent experiments performed in triplicate.

A, and 0.0083 ± 0.00004 μM and 0.025 ± 0.00021 μM for RSV-B, respectively (Table 1). This potent anti-RSV activity was not due to non-specific MEDS433 cytotoxicity since its cytotoxic concentration 50

Table 2
Analysis of the combination of MEDS433 and DPY against RSV-A replication.

MEDS433 concentration (fold of EC_{50}[a]) + 3 μM DPY	MEDS433 + DPY CI[b]	Drug combination effect of MEDS433 + DPY[c]
4x	0.192 ± 0.026	**Strong synergism**
2x	0.698 ± 0.034	**Synergism**
1x	0.657 ± 0.075	**Synergism**
0.5x	0.551 ± 0.042	**Synergism**
0.25x	0.493 ± 0.055	**Synergism**

[a] The EC_{50} values of MEDS433 were determined by PRAs in RSV-A-infected HEp-2 cells.
[b] Combination Index (CI), obtained by computational analysis with the CompuSyn software 1.0. Reported values represent means ± SD of data derived from $n = 3$ independent experiments in triplicate.
[c] Following the method of Chou (2006), drug combination effects are defined as: strong synergism for $0.1 < CI < 0.3$; synergism for $0.3 < CI < 0.7$.

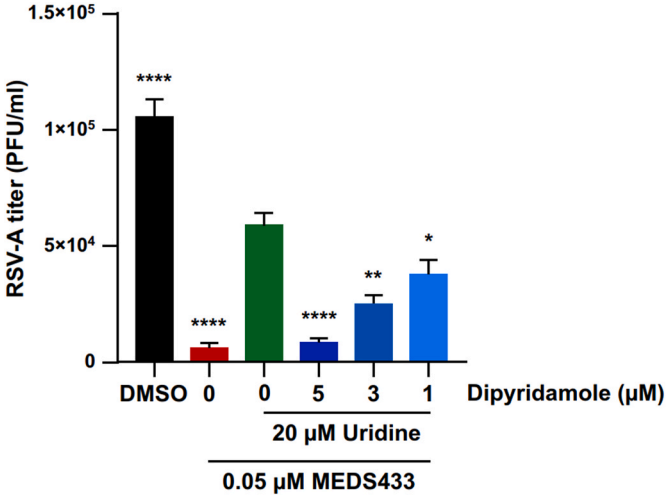

Fig. 6. A combination of modulators of pyrimidine metabolism inhibits RSV replication in the presence of exogenous uridine. PRAs were performed in HEp-2 cells treated with 0.05 μM MEDS433 alone, or in combination with different concentrations of DPY and 20 μM uridine prior to and during RSV-A infection (30 PFU/well). After virus adsorption, cells were incubated in the presence of compounds and at 72 h p.i., viral plaques were stained, and microscopically counted. Data shown are the means ± SD of $n = 3$ independent experiments performed in triplicate. Samples were analyzed by one-way ANOVA Dunnett's multiple comparison test. *, $p < 0.05$; **, $p < 0.005$; ****, $p < 0.0001$ compared to the calibrator sample (MEDS433 + 20 μM uridine, green column).

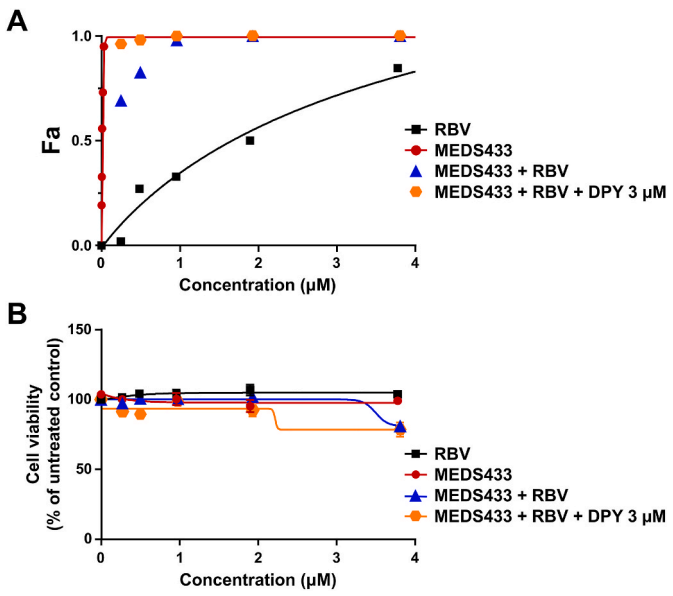

Fig. 7. Effects of the combination of MEDS433, RBV and DPY on RSV replication. (**A**) PRAs were performed in HEp-2 cell monolayers treated with different concentrations of MEDS433 and RBV as single agents, or in combination each other. Then, cells treated with MEDS433-RBV combination were also exposed to 3 μM of DPY prior to and during RSV-A infection (30 PFU/well). After virus adsorption, cells were incubated in the presence of compounds and, at 72 h p.i., viral plaques were stained and counted. Plaque numbers were analyzed by the CompuSyn software. The effects on RSV-A replication of MEDS433 or RBV used as single agents are depicted by red and black Fa curve, respectively. The effect of MEDS433-RBV or MEDS433-RBV-DPY combinations are indicated by blue triangles and orange hexagons, respectively. The results are representative of $n = 3$ independent experiments performed in triplicate. (**B**) To determine the cytotoxic effect of combinations, HEp-2 cells were treated with vehicle (DMSO), or with different concentrations of MEDS433 alone or in combination with different concentrations of RBV, and in the absence or presence of 3 μM of DPY. At 72 h, HEp-2 cell viability was assessed by the CellTiter-Glo Luminescent assay. Results are shown as means ± SD (error bars) of three independent experiments performed in triplicate.

(CC_{50}) for HEp-2 cells was of 84.30 ± 0.574 μM that produced positive Selectivity Index (SI) values of 10808 and 10157 for RSV-A and RSV-B, respectively (Table 1). Moreover, when compared with other *h*DHODH inhibitors, MEDS433 was slightly more effective than brequinar, a potent *h*DHODH inhibitor (Peters, 2018) endowed with a BSA activity against several human respiratory viruses (Sepúlveda et al., 2022; Zheng et al., 2022), inasmuch the EC_{50} of brequinar was 0.0113 ± 0.00005 μM and 0.0190 ± 0.00012 μM for RSV-A and RSV-B, respectively (Table 1). MEDS433, however, proved to be superior both to teriflunomide, the active metabolite of the clinically approved *h*DHODH inhibitor leflunomide endowed with an anti-RSV activity (Dunn et al., 2011), and to ASLAN003, a potent *h*DHODH inhibitor for which an antiviral activity against SARS-CoV-2 has recently been observed (Stegmann et al., 2022). In fact, the measured EC_{50} value of teriflunomide was 8.58 ± 0.309 μM against RSV-A and 6.54 ± 0.278 μM against RSV-B, while that of ASLAN003 was 0.59 ± 0.088 μM and 0.64 ± 0.029 μM for RSV-A and RSV-B, respectively (Table 1). Furthermore, it is noteworthy that MEDS433 was much more effective than RBV, because the measured EC_{50} for RBV was 2.3760 ± 0.0117 μM against RSV-A and 1.3264 ± 0.0105 μM against RSV-B (Table 1).

Then, to confirm the suitability of MEDS433 as an HTA candidate against RSV, the A549 cell line, as a second human airway epithelial cell model, was adopted to verify the anti-RSV activity in a different host cell system. Moreover, to leave aside the possibility that the inhibitory effect of MEDS433 stemmed from the type of antiviral assay, virus yield reduction assays (VRAs) were performed in A459 cells. As shown in Fig. 2 (panels D and E), even in A549 cells, MEDS433 exerted a potent anti-RSV activity with EC_{50} and EC_{90} values of 0.0381 ± 0.00022 μM and 0.136 ± 0.00089 μM for RSV-A, and of 0.0277 ± 0.00018 μM and 0.120 ± 0.00102 μM for RSV-B. Again, SI values were positive since in A549 cells the MEDS433 CC_{50} value was of 64.25 ± 3.125 μM, thus resulting in a SI of 1686 and 2319 for RSV-A and RSV-B, respectively (Table 1).

Overall, the results of these antiviral assays suggest a potent anti-RSV activity of MEDS433 in the low nanomolar range that was independent of the RSV strain used, the cell line, or the assay used.

3.3. *MEDS433 acts at a post-entry stage of RSV replicative cycle through the inhibition of viral RNA genome synthesis*

To identify the phase of the RSV replicative cycle targeted by MEDS433, time-of-addition (TOA) experiments were carried out by treating HEp-2 cells with MEDS433 (0.05 μM, 2 x EC_{90}) from −3 to −2 h prior to RSV-A infection (pretreatment, PRE-T); or during the infection (from −2 to 0 h p.i.; cotreatment, CO-T); or after virus adsorption (from 0 to 48 h p.i.; post-treatment, POST-T); or from −3 to 48 h p.i. (full-treatment, FULL-T). At 48 h p.i., infectious RSV-A particles released in cell supernatants were titrated by plaque assay. As depicted in Fig. 3A, MEDS433 did not affect neither the adsorption phase, nor the entry phase of RSV replication cycle. Conversely, it reduced significantly the production of infectious RSV particles of about two orders of magnitude, when added at a post-entry stage (POST-T) or left on cells from - 3 to 48 h p.i. (FULL-T). These results therefore indicated that the antiviral activity of MEDS433 derived from an interference with a synthetic stage of the RSV replication cycle that occurs after virus entry.

Thereafter, to further investigate the ability of MEDS433 to interfere with RSV replication, the effect of the *h*DHODH inhibitor on the synthesis of RSV genome was investigated at various times p.i. by qRT-PCR. Fig. 3B shows that in comparison to DMSO-treated cells, the addition of

Table 3
Analysis of the effects of the combination of MEDS433, RBV and DPY against RSV-A replication.

MEDS433+RBV combination at equipotent ratio (fold of EC_{50}[a])	MEDS433+RBV CI[b]	Drug combination effect of MEDS433+RBV[c]	MEDS433+RBV + 3 μM DPY CI[d]	Drug combination effect of MEDS433+RBV+3 μM DPY[c]
4x	0.435 ± 0.053	**Synergism**	0.425 ± 0.072	**Synergism**
2x	0.214 ± 0.027	**Strong synergism**	0.213 ± 0.036	**Strong synergism**
1x	0.573 ± 0.042	**Synergism**	0.106 ± 0.018	**Strong synergism**
0.5x	0.646 ± 0.118	**Synergism**	0.287 ± 0.373	**Strong synergism**
0.25x	0.424 ± 0.045	**Synergism**	0.182 ± 0.032	**Strong synergism**

[a] Fold of EC_{50} MEDS433/EC_{50} RBV yielding an equipotent concentration ratio (approximately 1:0.008) between the two combined drugs. The EC_{50} values was determined by PRAs against RSV-A in HEp-2 cells.

[b] Combination Index (CI), extrapolated by computational analysis with the CompuSyn software. Reported values represent means ± SD of data derived from $n = 3$ independent experiments in triplicate using MEDS433+RBV concentration ratio as showed in[a].

[c] Drug combination effect defined as: strong synergism for $0.1 < CI < 0.3$; synergism for $0.3 < CI < 0.7$, according to the method of Chou (2006).

[d] Combination Index (CI), extrapolated by computational analysis with the CompuSyn software. Reported values represent means ± SD of data derived from $n = 3$ independent experiments in triplicate using MEDS433+RBV concentration ratio showed in [a] and added with 3 μM of DPY for each combination.

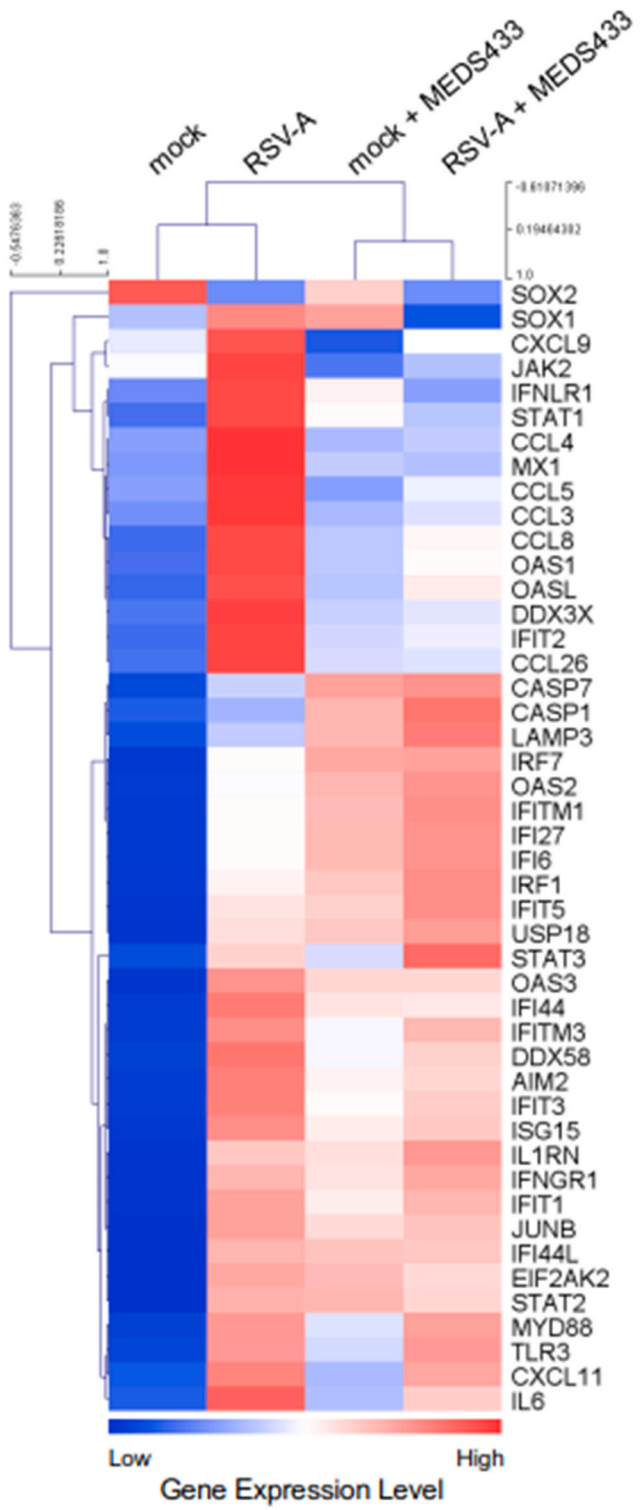

Fig. 8. MEDS433 and RSV infection upregulate the expression of Interferon-Stimulated Genes (ISGs). HEp-2 cell monolayers were treated with 1 μM MEDS433 or DMSO for 16 h, and then, where indicated, cells were infected with RSV-A at an MOI of 1 in presence of the compound for 24 h. Thereafter, mRNA was purified, labeled and hybridized to human gene expression microarrays. After hybridization, slide scanning, and image analysis, expression values, reported as log2 intensities, were normalized and replicated measurements averaged. Unsupervised hierarchical clustering, with Pearson's correlation as distance metrics, was applied to the expression profiles of ISGs and innate immune genes in the 4 experimental conditions, using standardized log2 intensities.

MEDS433 (0.05 μM) almost suppressed completely the accumulation of RSV genomes throughout the entire timeframe of RSV replication that was evaluated, thus suggesting that indeed it hindered the synthesis of new viral RNA genomes. Similar results were obtained in HEp-2 cells infected with RSV-B (data not shown).

These results thus identify inhibition of viral RNA replication as a mechanism of antiviral activity of MEDS433 against RSV, and allow to hypothesize that it may stem from depletion or imbalance of pyrimidine pools caused by the inhibition of *h*DHODH activity.

3.4. The anti-RSV activity of MEDS433 derives from specific inhibition of the novo pyrimidine biosynthesis

To verify the above hypothesis, we investigated whether the antiviral activity of MEDS433 against RSV could be affected by the addition of increasing concentrations of exogenous uridine or cytidine, as final products of the *de novo* pyrimidine pathway. As shown in Fig. 4A, RSV-A replication in HEp-2 cells was gradually rescued by the addition of increasing amounts of both uridine and cytidine, thus indicating that the *de novo* pyrimidine biosynthesis pathway was inhibited by MEDS433 in RSV-infected cells.

To further confirm that MEDS433 antiviral activity derived from its ability to block *h*DHODH enzymatic function, RSV-A-infected HEp-2 cells were exposed to MEDS433 in the presence of increasing concentrations of orotic acid (ORO) or dihydroorotic acid (DHO), as the specific *h*DHODH product or substrate, respectively. As depicted in Fig. 4B, only the addition of ORO reversed the antiviral activity of MEDS433, while that of DHO, even at 20,000-fold excess the MEDS433 concentration used (0.05 μM), did not affect the inhibitory effect of MEDS433.

Taken together, these results clearly indicated that the MEDS433-mediated suppression of RSV genome replication (Fig. 3B), derived from a specific inhibition of the *h*DHODH enzymatic activity in RSV-infected cells that prevents the oxidation of DHO to ORO in the *de novo* biosynthesis of pyrimidines.

3.5. The combination of MEDS433 with an inhibitor of the pyrimidine salvage pathway is effective against RSV even in the presence of uridine

Since we observed that addition of exogenous uridine reversed the anti-RSV activity of MEDS433, it could be possible that its physiological plasma concentration in the host reduces the antiviral activity of MEDS433 through the salvage pathway. To consider this problem, we investigated the effect of the combination of MEDS433 with dipyridamole (DPY), an inhibitor of the nucleoside transporters hENT1 and 2 implicated in the pyrimidine salvage pathway (Fitzgerald, 1987; Ward et al., 2000; Schaper, 2005). For this purpose, PRAs were performed in RSV-A-infected HEp-2 cells to assess the effect of the combination of a 0.25-, 0.5-, 1-, 2-, or 4-fold of MEDS433 EC_{50} to 3 μM DPY. Fig. 5A shows the consequence of MEDS433-DPY combination as a fractional effect analysis (Fa) plot relative to the compound concentrations, where Fa values closer to 1 indicate greater antiviral activity. It's to be noted that DPY did not exert any inhibitory activity on RSV-A replication when used as a single agent, even tested up to 12 μM (Fig. 5 and data not shown). Nevertheless, when 3 μM DPY was used in combination with different concentrations of MEDS433, it increased the anti-RSV activity of the *h*DHODH inhibitor (Fig. 5A, blue squares); in fact, the EC_{50} of MEDS433 (0.0085 ± 0.00003 μM) was reduced to 0.0013 ± 0.000004 μM by the combination with DPY. As reported in Table 2, values of the computed combination index (CI) (Chou and Martin, 2005; Chou, 2006) confirmed that the combination of MEDS433 with DPY resulted in a synergistic antiviral activity at any of the MEDS433 concentrations tested, since all the CIs were <0.7. Moreover, the DPY-mediated increase of MEDS433 antiviral activity was not due to an aspecific cytotoxic effect, since none of the combinations examined affected HEp-2 cell viability (Fig. 5B).

Then, we examined whether the MEDS433-DPY synergistic

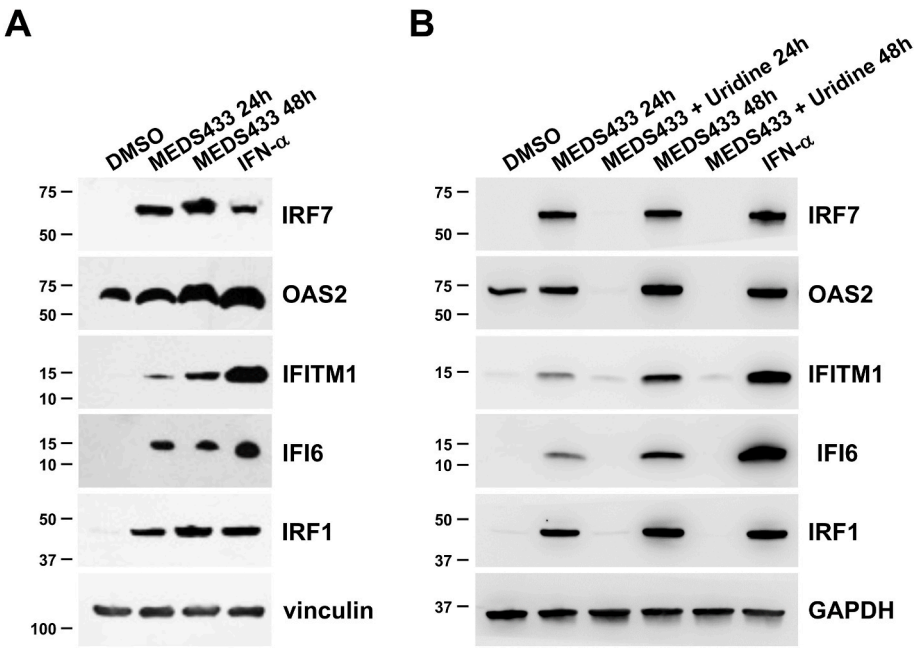

Fig. 9. MEDS433-induced ISG proteins expression depends on pyrimidine depletion. HEp-2 cells were treated with DMSO or with 1 μM MEDS433 for 24 or 48 h in the absence (**A**) or presence of uridine (1 mM) (**B**). Cells treated with IFN-α (100 ng/ml) for 24 h served as a positive control for ISG proteins expression. Then, total cell protein extracts were prepared, fractionated by 4–15% SDS-PAGE, and analyzed by immunoblotting with anti-IRF7, anti-OAS2, anti-IFITM1, anti-IFI6, or anti-IRF1 Abs. Vinculin or GAPDH immunodetection was used as a control for protein loading. Molecular weight markers are shown at the left side of each panel.

combination could be effective even in the presence of a hyper-physiological concentration of uridine (20 μM), far exceeding the plasma concentrations (Pizzorno et al., 2002). As shown in Fig. 6, the presence of exogenous uridine reversed, as expected, the inhibitory activity of 0.05 μM MEDS433 that suppressed RSV-A replication when tested as a single agent (Fig. 2B). To the contrary, addition of increasing amounts of DPY renovated the inhibitory activity of MEDS433, therefore suggesting the suitability of this combination to inhibit RSV replication, even in the presence of exogenous uridine, as occurring in the host.

3.6. MEDS433 and RBV act synergistically against RSV replication

Next, we investigated whether the anti-RSV activity of MEDS433 and RBV, to date the only drug approved for the treatment of severe RSV infections, could produce additive, synergistic, or antagonistic effect when examined in combination. For this purpose, PRAs were performed with different concentrations of both MEDS433 and RBV corresponding to 0.25-, 0.5-, 1-, 2-, or 4-fold of their EC_{50} values to obtain equipotent ratios (MEDS433 EC_{50}/RBV EC_{50}). Fig. 7A shows that the anti-RSV effectiveness of RBV was clearly increased by the combination with MEDS433 as shown by FA values (blue triangles) closer to 1 than those of RBV when used as a single agent. Accordingly, the EC_{50} of RBV (1.6652 ± 0.0034 μM when used as a single agent) was reduced to < 0.235 μM by the addition of the *h*DHODH inhibitor. The synergism between RBV and MEDS433 was confirmed by the computed CI values < 0.7 at any of the MEDS433 to RBV combination tested (Table 3).

Then, to evaluate the efficacy of the MEDS433-RBV combination in the background of a DPY treatment able to hamper the pyrimidine salvage pathway, the combination of different MEDS433 EC_{50} to RBV EC_{50} was measured in the presence of 3 μM DPY. As reported in Fig. 7A and Table 3, the anti-RSV activity of the MEDS433-RBV combination was further enhanced by the addition of DPY, since the FA values of the triple combination (orange hexagons) were even more close to 1 than those of the MEDS433-RBV combination, and the EC_{50} of RBV further reduced to < 0.235 μM.

Furthermore, excluding concentrations of MEDS433-RBV higher than 2 μM for which weak cytotoxicity was observed, none of the other MEDS433-RBV-DPY combinations exhibited significant cytotoxic effects against HEp-2 cells (Fig. 7B), thus indicating that their synergistic anti-RSV activity was not the result of an increased cytotoxicity, which would have prevented the virus from replicating, but that it derived from the combined interference of different targets and mechanisms of action.

Together, these results suggest that the combination of MEDS433 with RBV and that of MEDS433, RBV and DPY might be of interest to design a new pharmacological strategy to be considered for the control of RSV infections.

3.7. MEDS433 stimulates the expression of ISG proteins that contribute to the antiviral activity against RSV

Since a link between inhibition of pyrimidine biosynthesis and enhanced expression of Interferon-Stimulated Genes (ISGs) has been observed for some *h*DHODH inhibitors (Lucas-Hourani et al., 2013; Cheung et al., 2017; Zheng et al., 2022), we investigated whether MEDS433 was able to regulate ISGs expression that, in turn, may contribute to the overall anti-RSV activity of the *h*DHODH inhibitor. To this end, gene expression profiling by microarray was performed to detect changes in a set of ISGs and host innate immune genes after RSV-A infection and/or MEDS433 treatment of HEp-2 cells. As shown in Fig. 8, host genes involved in the Interferon (IFN) pathway were clearly upregulated by RSV infection, including STAT1, MX1 and OAS1, as well as some inflammatory chemokines, such as CCL3 (MIP-1α), CCL4 (MIP-1β), and CCL5 (RANTES). Noteworthy, expression of these virus-induced inflammatory chemokines, as well as of IL6, was reduced by MEDS433 treatment of RSV-infected cells. However, the most intriguing finding was the ability of MEDS433 to stimulate the expression of some ISGs that were not upregulated by RSV infection, such as IRF7, OAS2, IFITM1, IFI27, IFI6, and IRF1. Interestingly, the expression of these MEDS433-induced ISG remained elevated even in MEDS433-treated and RSV-infected cells (Fig. 8). This finding was then validated at the protein level (Fig. 9A), thus confirming that MEDS433 induced these antiviral ISG proteins independently of RSV infection. Moreover, supplementation with exogenous uridine reversed extensively the induction of the ISG proteins by MEDS433 (Fig. 9B), hence sustaining a functional

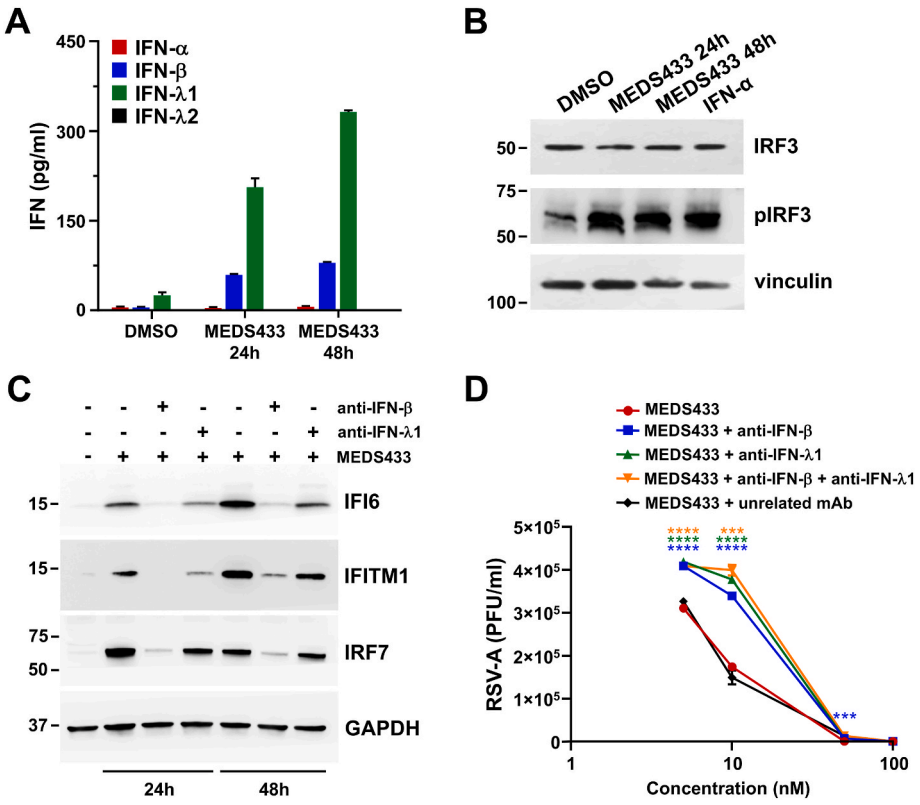

Fig. 10. The MEDS433-induced secretion of IFN-β and IFN-λ1 is required for the stimulation of ISG proteins and the anti-RSV activity. (**A**) MEDS433 treatment induces the production of type-I and type-III IFNs. HEp-2 cells were exposed to DMSO or 1 μM MEDS433 for 24 or 48 h. Cell culture medium was subjected to either IFN-α and IFN-β, IFN-λ1, or IFN-λ2 ELISA to measure IFNs. Data shown are the means ± SD (error bars) of two independent experiments performed in triplicate. (**B**) MEDS433 stimulates the phosphorylation of IRF3. HEp-2 cells were treated with DMSO, or with 1 μM MEDS433 for 24 or 48 h, or with IFN-α (100 ng/ml) for 24 h. Total cell protein extracts were then prepared and analyzed by immunoblotting with anti-IRF3 or anti-phospho-IRF3 mAbs. Vinculin immunodetection was used as a control for protein loading. Molecular weight markers are shown at the left side of each panel. (**C**) Neutralization of IFN-β or IFN-λ1 reduces the accumulation of MEDS433-induced ISG proteins. HEp-2 cells were left untreated or treated with 1 μM MEDS433 for 24 or 48 h in the absence or presence of neutralizing mAbs against IFN-β (10 μg/ml) or IFN-λ1 (10 μg/ml). Then, total cell protein extracts were prepared, and analyzed by immunoblotting with anti-IFI6, IFITM1, or IRF7 Abs. GAPDH immunodetection was used as a control for protein loading. Molecular weight markers are shown at the left side of each panel. (**D**) Neutralization of IFN-β or IFN-λ1 decreases the strength of the antiviral activity of MEDS433 against RSV. VRAs were performed in HEp-2 cell monolayers infected with RSV-A and treated with increasing concentrations of MEDS433 1 h before, during, and post-infection, and in the presence or absence of neutralizing mAbs against IFN-β (10 μg/ml) or IFN-λ1 (10 μg/ml), or an unrelated murine mAb (10 μg/ml). At 72 h p.i., cell supernatants were harvested, and titrated by the plaque assay in HEp-2 cells. Data shown are the means ± SD of $n = 2$ independent experiments performed in triplicate and analyzed by two-way ANOVA Dunnett's multiple comparison test. ***, $p < 0.001$; ****, $p < 0.0001$ compared to the calibrator sample (MEDS433 alone).

relationship existing between stimulation of ISGs expression and inhibition of pyrimidine biosynthesis.

To investigate the mechanism by which MEDS433 upregulated the expression of ISG proteins in the absence of an external interferon inducer, such as RSV infection, we examined whether the *h*DHODH inhibitor could directly induce type I and/or type III Interferons (IFNs) production. To this end, ELISA were performed to detect IFNs in the supernatants of HEp-2 cells stimulated with MEDS433. As shown in Fig. 10A, MEDS433 induced the secretion of large amounts of IFN-λ1 and, to a lesser extent, of IFN-β, while neither any of the human IFN-α subtypes, nor IFN-λ2 were detected by ELISA in the supernatants of MEDS433-treated cells. In this regard, transcription of the IFN-β gene requires the activation of the constitutive transcription factor IRF3, while that of IFN-λ1 gene requires activated IRF3-IRF7 heterodimers (Negishi et al., 2018). Since we observed that IRF7 is induced by MEDS433 (Fig. 9), we hypothesized that the *h*DHODH inhibitor could induced the activation of the early regulator IRF3 and thus IFN-β gene transcription; then, secreted IFN-β, in an autocrine manner, could induce IRF7 and, as a consequence, activated the expression of IFN-λ1. Indeed, MEDS433 proved able to stimulate IRF3 phosphorylation (Fig. 10B), thus sustaining its ability to directly induce IFN-β gene transcription.

Then, to evaluate the contribution of secreted IFN-β and IFN-λ1 in the upregulation of ISG proteins expression, the content of IF6, IFITM1 and IRF7 proteins was measured in HEp-2 cells exposed to MEDS433 in the presence of neutralizing mAbs directed against IFN-β or IFN-λ1. As depicted in Fig. 10C, the presence of neutralizing antibodies reduced the levels of all examined ISG proteins, thus confirming that stimulation of ISG proteins expression was a consequence of MEDS433-induced secretion of IFN-β and IFN-λ1.

To further confirm the importance of secreted type I IFNs in the overall anti-RSV activity of MEDS433, VRAs were performed in HEp-2 cells infected with RSV-A in the absence or presence of neutralizing mAbs against IFN-β or IFN-λ1. Fig. 10D shows that the neutralization of IFN-β, IFN-λ1, or both decreased significantly the inhibitory activity of MEDS433. In fact, its EC_{50} value (0.0086 ± 0.00003 μM) was raised to 0.0189 ± 0.00052 μM by the anti-IFN-β mAb, 0.0214 ± 0.00077 μM by the anti-IFN-λ1 mAb, and 0.0233 ± 0.00038 by the addition of both mAbs. These results therefore sustain a contribution of the activated IFN pathway in the overall antiviral activity of MEDS433 against RSV.

Then, to investigate the relevance of these MEDS433-induced ISG proteins in the overall anti-RSV activity of the *h*DHODH inhibitor, a doxycycline-regulated expression system was developed for efficient expression of IFI6, IFITM1, or IRF7 in HEp-2 cells through their

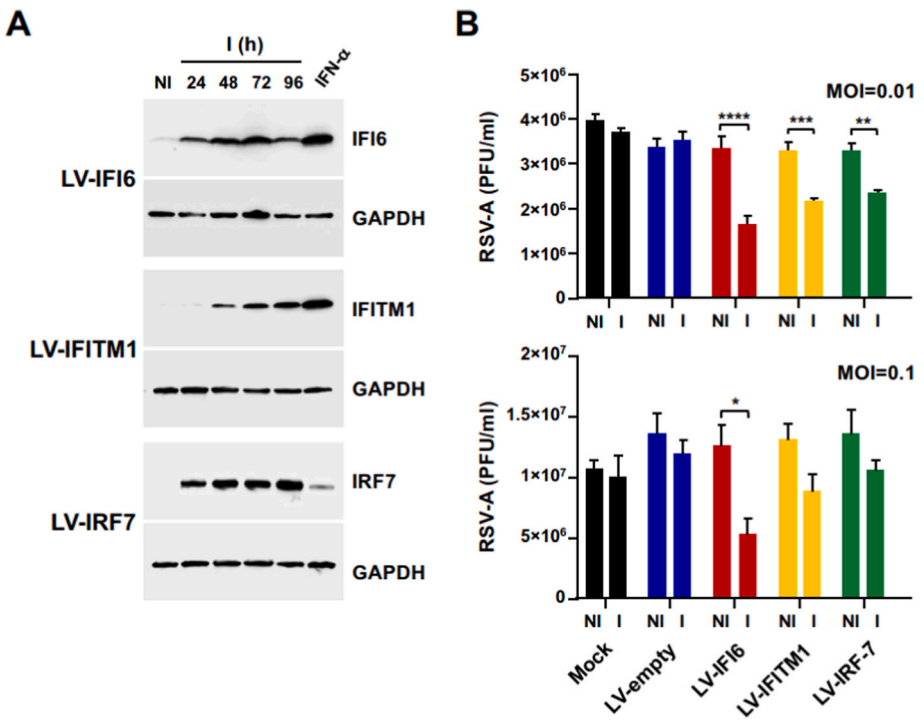

Fig. 11. Inducible expression of IFI6, IFITM1 or IRF7 proteins hampers RSV-A replication. (**A**) Doxycycline-inducible expression of IFI6, IFITM1 and IRF7 in HEp-2-derived cells lines LV-IFI6, LV-IFITM1, and LV-IRF7. Protein extracts were from not-induced (NI) cells, or from cells exposed to doxycycline (100 ng/ml) for 24, 48, 72, or 96 h. Extracts from NI cells exposed to IFN-α (100 ng/ml) for 24 h were used as a positive control for ISG protein expression. GAPDH immunodetection was used as a control for protein loading. (**B**) Replication of RSV-A is affected by the inducible expression of IFI6, IFITM1, or IRF7. LV-empty, LV-IF6, LV-IFITM1, and LV-IRF7 cells were left untreated or treated with doxycycline (100 ng/ml) 24 h prior to infection with RSV-A at MOI of 0.01 or 0.1. At 72 h p.i., supernatants were harvested, and titrated for RSV infectivity in HEp-2 cells. The data shown are the means ± SD of $n = 2$ independent experiments performed in triplicate and analyzed by a two-way ANOVA followed by Sidak's multiple comparison test compared to the corresponding NI sample. *, $p < 0.05$; **, $p < 0.005$; ***, $p < 0.001$; ****, $p < 0.0001$.

transduction with Tet-One lentiviral vectors (LV) containing the corresponding ISG ORFs. As reported in Fig. 11A, the doxycycline-inducible expression of IFI6, IFITM1, and IRF7, was confirmed by immunoblotting in LV-transduced cell lines up to 96 h of antibiotic stimulation. RSV-A replication was then examined in these cell lines, in the absence of MEDS433 treatment; in comparison to mock-transduced HEp-2 cells or cells transduced with an empty LV (LV-empty), the doxycycline-induced expression of all ISG proteins affected RSV-A yield, with a maximum reduction rate of more than 2-fold for cells expressing IFI6 (Fig. 11B).

Taken as a whole, the results of this section indicate as a second mechanism of the antiviral activity of MEDS433 against RSV, its ability to stimulate the activation of the IFN pathway, through induction of IFN-β and IFN-λ1 secretion that, in turn, upregulates the expression of antiviral ISG proteins able to exert a functional role in hindering RSV replication.

3.8. *MEDS433 inhibits RSV-A replication in a mucociliated human small airway epithelium model*

Lastly, the anti-RSV activity of MEDS433 was investigate in primary human bronchiolar epithelial tissues maintained at the air-liquid interface. This cell system represents a valuable model to assess both toxicity and efficacy of candidate antiviral agents in an *ex vivo* system that recapitulates the lining of human lung small airway, including ciliated and goblet cells that produce cilia movement and mucus (Hasan et al., 2018). As shown in Fig. 12A, treatment of the small airway epithelium with 1 μM MEDS433 after RSV-A infection, already at 24 h p.i., caused a significant reduction of the RSV yield released compared to untreated and RSV-infected cultures (RSV-A). The extent of the inhibitory effect of MEDS433 was more pronounced from 48 h p.i. and up to 96 h p.i. Indeed, when epithelia were exposed to higher concentrations of MEDS433 (5 or 10 μM), the inhibition of the release of RSV infectious particles was even more severe and quantified as more than 2 orders of magnitude (Fig. 12A). The antiviral activity of MEDS433 in this *ex vivo* respiratory epithelium model was not due to non-specific cytotoxicity, since LDH levels measured in the basal medium of MEDS433-treated cultures were comparable to that of untreated mock-infected epithelium (Mock) (Fig. 12B). These results were further confirmed by histological analysis. In fact, as depicted in Fig. 12C, mock-infected MEDS433-treated epithelia (*Middle and Lower left* panels) showed a healthy appearance, with intact cilia and an unaltered histological structure compared to the untreated mock-infected epithelium (Mock) (Fig. 12C, *Upper left*). RSV infection, as expected, caused severe tissue damages characterized by cilia disappearance and thinning of the epithelial layer (RSV-A) (Fig. 12C, *Upper right*). However, when small airway epithelia were treated with MEDS433 after RSV infection, their histological structure was protected, and tissues appeared healthy at 96 h p.i. (Fig. 12C, *Middle and Lower right* panels).

Together, these results confirm that MEDS433 exerted an anti-RSV activity even in an *ex vivo* model of human respiratory epithelium.

4. Discussion

To replicate efficiently in human cells, viruses requires the contribution of host cell *h*DHODH, as we reaffirmed here for RSV (Fig. 1). Therefore, its enzymatic activity is a reliable HTA target to develop new broad-spectrum antivirals (Zheng et al., 2022). To further support such perspective, in this study, we have characterized the anti-RSV activity of MEDS433, a novel *h*DHODH inhibitor. The observed results suggest that the overall antiviral activity of MEDS433 against RSV derives from both the selective inhibition of *h*DHODH activity in RSV-infected cells that causes pyrimidine depletion and the consequent suppression of RSV

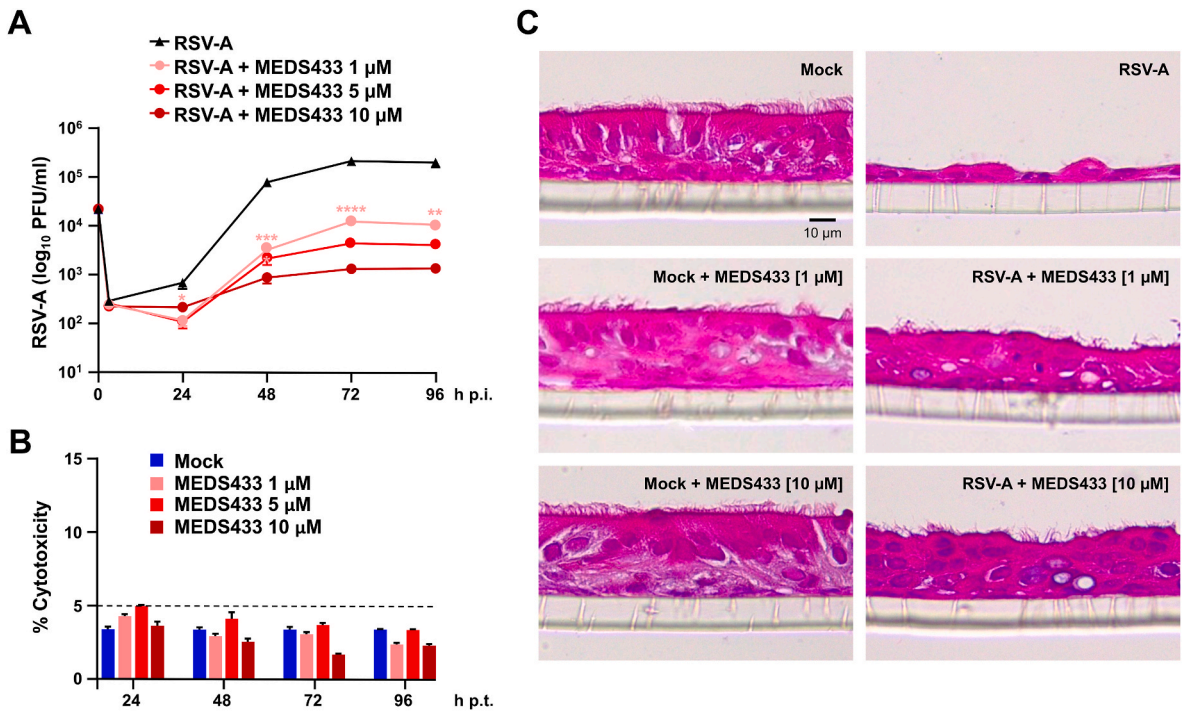

Fig. 12. MEDS433 inhibit RSV replication in a human mucociliated small airway epithelium model (**A**) Bronchiolar epithelia were treated with different concentrations of MEDS433 (1, 5 and 10 μM) in the basolateral (BL) medium for 1 h at 37 °C before infection. Then, small airway epithelia were infected apically with RSV-A at an MOI of 0.02 in presence of MEDS433 for 3h at 37 °C. After viral absorption, the inoculum was removed, and MEDS433 was applied in the BL medium. Viral progeny was harvested from the apical surface at 24, 48, 72, and 96 h p.i. and titrated by the plaque assay in HEp-2 cells. The data shown are the means ± SD of $n = 2$ independent experiments performed in duplicate and analyzed by a two-way ANOVA, followed by Dunnett's multiple comparison test. Statistical analysis was performed by comparing the RSV-A-infected sample (RSV-A) with the MEDS433-treated and RSV-infected tissues for each time. Statistical significance is shown only for RSV-A+MEDS433 1 μM samples. *, $p < 0.05$; **, $p < 0.005$; ****, $p < 0.0001$. (**B**) To determine the cytotoxic effect of the different concentrations of MEDS433, at each time-point post-treatment (p.t.) the basal medium was harvested and the released LDH was measured by the LDH-Glo Cytotoxicity assay. Results are expressed as % cytotoxicity and as means ± SD (error bars) of two independent experiments performed in duplicate. The threshold limit 5% of the toxicity index indicates the physiological cell turnover in this airway epithelium model. (**C**) Transversal cross sections of small airway epithelia stained at 96 h p.i. Representative histological images of mock-infected (Mock, *Left*), MEDS433-treated and mock-infected (Mock+MEDS433, *Left*), RSV-infected (RSV-A, *Right*), or MEDS433-treated and RSV-infected epithelia (RSV-A+MEDS433, *Right*) are shown. Slides were prepared from epithelia stained with hematoxylin-eosin. Magnification: 40 × . Scale bar for each image: 10 μm.

genome synthesis, as well as the activation of antiviral ISG proteins that hamper RSV replication.

These results confirm the viability of *h*DHODH pharmacological targeting to develop anti-RSV agents, as previously reported for other *h*DHODH inhibitors, such as leflunomide (Dunn et al., 2011), FA-613 (Cheung et al., 2017), and RYL-634 (Yang et al., 2019). However, it is worth noting that our study adds a couple of new pieces of knowledge that may be relevant to develop further pyrimidine synthesis inhibitors against RSV infections.

The first pertains to the observation that a combination between MEDS433 and DPY, an inhibitor of the pyrimidine salvage pathway, was synergistic against RSV replication (Fig. 5A), even in the presence of uridine concentration higher than physiological plasma concentration (Fig. 6). In fact, despite that DPY is lacking anti-RSV activity (Fig. 5), when combined with MEDS433, it restored the antiviral activity of a concentration of MEDS433 no longer effective in presence of uridine (Fig. 6). This observation is relevant, inasmuch poor effectiveness has been reported for some *h*DHODH inhibitors in the treatment of infections by RNA viruses in both rodents and non-human primate models, despite their *in vitro* efficacy (Wang et al., 2011; Smee et al., 2012; Grandin et al., 2016). It has been speculated that this failure could depend on an insufficient antiviral potency or poor pharmacokinetics of the evaluated DHODH inhibitor, and/or on the compensating effect of the host pyrimidine salvage pathway through the import of exogenous uridine into virus-infected cells (Zheng et al., 2022). Accordingly, the pharmacological targeting of the pyrimidine salvage pathway may be beneficial, as it may enhance the *in vivo* antiviral efficacy of DHODH inhibitors.

DPY is a pyrimidopyrimidine derivative that inhibits ENT 1 and 2, the most effective nucleoside transporters of the pyrimidine salvage pathway (Fitzgerald, 1987; Ward et al., 2000), and an antiplatelet agent approved for the prophylaxis of thromboembolism in cardiovascular diseases (Schaper, 2005). However, the combination of DPY and *h*DHODH inhibitors against viral infections is at a very early stage and is still understudied. In this regard, we have observed that the combination of DPY with MEDS433 was effective against HSV-1, SARS-CoV-2, and influenza A virus, even in the presence of a hyper-physiological concentration of uridine (Luganini et al., 2021; Calistri et al., 2021; Sibille et al., 2022). Importantly, the concentration of DPY (3 μM) synergic with MEDS433 against RSV replication (Fig. 6) is lower than the DPY Cmax (2.2 μg/mL, which corresponds to 4.4 μM) (Gregov et al., 1987) and, thus, clinically achievable in patients undergoing DPY therapy. The wide clinical experience of DPY could allow its rapid repositioning even against respiratory virus infections, including RSV, to be clinically advantageous in combination with *h*DHODH inhibitors.

A second point worth discussing concerns the ability of MEDS433 to stimulate the expression of ISG proteins that hamper RSV replication (Fig. 11). Although it has been previously reported that *h*DHODH inhibitors induce ISGs expression (Lucas-Hourani et al., 2013; Cheung et al., 2017; Luthra et al., 2018), this is the first observation, to our knowledge, that a *h*DHODH inhibitor stimulates the expression of antiviral ISG proteins, such as IFI6, IFITM1 I and IRF7, which reduce

RSV replication when expressed in isolation (Fig. 11B), and previously observed to affect the virus (McDonald et al., 2016; Smith et al., 2019). Our results therefore functionally sustain the view that the antiviral activity of *h*DHODH inhibitors depends on both the pyrimidine depletion that halts the activity of viral polymerases, and the induction of protein effectors of the innate antiviral response (Lucas-Hourani et al., 2013). Although the mechanisms underlying the activation of ISGs following inhibition of pyrimidine biosynthesis remain to be well-defined, it has been hypothesized that the cellular stress associated to nucleoside deprivation fosters expression of ISGs that, in turn, contribute to the establishment of an antiviral state to infections by RNA viruses (Zheng et al., 2022). In this regard, we observed that the induction of ISG proteins by MEDS433 is linked to depletion of pyrimidines, as uridine supplementation prevented their expression in cells exposed to the *h*DHODH inhibitor (Fig. 9B). Moreover, different pathways of ISGs activation have been suggested for different *h*DHODH inhibitors (Zheng et al., 2022), since the dependency from type I IFNs production has been reported for FA613 (Cheung et al., 2017), while an IFN-independent mechanism has been observed for DD264, brequinar, and SW835 (Lucas-Hourani et al., 2013; Luthra et al., 2018). Here, we have observed that the MEDS433-mediated induction of IFI6, IFITM1, and IRF7 proteins requires secretion of IFN-β and IFN-λ1, as their neutralization reduces the accumulation of these ISG proteins in MEDS433-treated cells (Fig. 10C). Since neutralization of IFN-β and IFN-λ1 reduced the anti-RSV activity of MEDS433 as well (Fig. 10D), activation of the IFN pathway and ISG proteins expression indeed contribute to the overall anti-RSV activity of MEDS433.

Interestingly, activation of IRF1, through the DNA damage response kinase ATM, has been observed to occur in HEK293T cells for the SW835-mediated and IFN-independent ISGs stimulation (Luthra et al., 2018). Although IRF1 was induced even by MEDS433 in HEp-2 cells (Fig. 9), a role of this transcription factor in the ISGs stimulation, in the context of the IFN-dependent mechanism triggered by MEDS433, remains to be defined. In this study, we have observed the ability of MEDS433 to stimulate the phosphorylation of constitutive IRF3 (Fig. 10B), as an essential step in its activation that leads up to IFN-β gene transcription (Negishi et al., 2018). Although further investigations are required to fully elucidate the mechanism(s) of the IFN-dependent ISGs stimulation by MEDS433 (i.e., activation of the transduction pathways upstream from IRF3 phosphorylation), our observations provide novel insights toward the development of pyrimidine synthesis inhibitors to modulate the innate antiviral response.

Moreover, it should be emphasized, as an important added value of MEDS433, its broad-spectrum antiviral efficacy against different human viruses that cause RTIs. In fact, in addition to RSV, we have observed the ability of MEDS433 to inhibit the replication of influenza A and B viruses (Sibille et al., 2022), as well as of coronaviruses, such as hCoV-229E, hCoV-OC43, and SARS-CoV-2 (Calistri et al., 2021). Indeed, this trait and the inherent HTA advantage of the low risk of emergence of drug resistance, make MEDS433 of interest for the development of new BSA agents, even in the preparedness against future emerging human respiratory viruses, given the independence of its antiviral effects with respect to a specific virus.

5. Conclusions

In conclusion, this study suggests MEDS433 as an attractive novel anti-RSV HTA candidate endowed with advantageous features, such as a very potent antiviral activity, its amenability to combination regimens with both nucleoside analogues and other anti-pyrimidines, such as RBV and DPY, as well as its ability to trigger protein effectors of the innate antiviral response. The potent *in vitro* anti-RSV activity of MEDS433 and its valuable drug-like profile now ensure further studies to evaluate its efficacy in preclinical animal models of RSV infection.

Declaration of competing interest

The authors declare that they have no known competing financial interests or personal relationships that could have appeared to influence the work reported in this paper.

Data availability

Data will be made available on request.

Acknowledgements

This work was supported by EU funding within the MUR PNRR Extended Partnership initiative on Emerging Infectious Diseases (Project no. PE00000007, INF-ACT) to G.G.; the Italian Ministry for Universities and Scientific Research (Research Programs of Significant National Interest, PRIN 2017–2020, Grant No. 2017HWPZZZ_002) to A.L.; Piedmont Region (PAR FSC INFRA-P2 B COVID) to M.L.L., G.C., and G.G.; NATO SPS Grant. No. G5937 to M.L.L. and G.G.; and the University of Torino (Ricerca Locale) to A.L., D.B., M.L.L., and G.G.

References

Amarelle, L., Lecuona, E.A., 2018. Nonhospitable host: targeting cellular factors as an antiviral strategy for respiratory viruses. Am. J. Respir. Cell Mol. Biol. 59, 666–667. https://doi.org/10.1165/rcmb.2018-0268ED.

Beaird, O.E., Freifeld, A., Ison, M.G., Lawrence, S.J., Theodoropoulos, N., Clark, N.M., Razonable, R.R., Alangaden, G., Miller, R., Smith, J., Young, J.A.H., Hawkinson, D., Pursell, K., Kaul, D.R., 2016. Current practices for treatment of respiratory syncytial virus and other non-influenza respiratory viruses in high-risk patient populations: a survey of institutions in the Midwestern Respiratory Virus Collaborative. Transpl. Infect. Dis. 18, 210–215. https://doi.org/10.1111/tid.12510.

Boschi, D., Pippione, A.C., Sainas, S., Lolli, M.L., 2019. Dihydroorotate dehydrogenase inhibitors in anti-infective drug research. Eur. J. Med. Chem. 183, 111681 https://doi.org/10.1016/j.ejmech.2019.111681.

Broadbent, L., Groves, H., Shields, M.D., Power, U.F., 2015. Respiratory syncytial virus, an ongoing medical dilemma: an expert commentary on respiratory syncytial virus prophylactic and therapeutic pharmaceuticals currently in clinical trials. Influenza Other Resp. Viruses. 9, 169–178. https://doi.org/10.1111/irv.12313.

Calistri, A., Luganini, A., Mognetti, B., Elder, E., Sibille, G., Conciatori, V., Del Vecchio, C., Sainas, S., Boschi, D., Montserrat, N., Mirazimi, A., Lolli, M.L., Gribaudo, G., Parolin, C., 2021. The new generation hDHODH inhibitor MEDS433 hinders the in vitro replication of SARS-CoV-2 and other human coronaviruses. Microorganisms 9, 1731. https://doi.org/10.3390/microorganisms9081731.

Cheung, N.N., Lai, K.K., Dai, J., Kok, K.H., Chen, H., Chan, K.H., Yuen, K.Y., Kao, R.Y.T., 2017. Broad-spectrum inhibition of common respiratory RNA viruses by a pyrimidine synthesis inhibitor with involvement of the host antiviral response. J. Gen. Virol. 98, 946–954. https://doi.org/10.1099/jgv.0.000758.

Chou, T.C., 2006. Theoretical basis, experimental design, and computerized simulation of synergism and antagonism in drug combination studies. Pharmacol. Rev. 58, 621–681. https://doi.org/10.1124/pr.58.3.10.

Chou, T.C., Martin, N., 2005. CompuSyn for Drug Combinations: PC Software and User's Guide: a Computer Program for Quantitation of Synergism and Antagonism in Drug Combinations, and the Determination of IC_{50} and ED_{50} and LD_{50} Values. ComboSyn Inc., Paramus, NJ. https://www.combosyn.com.

Coelho, A.R., Oliveira, P.J., 2020. Dihydroorotate dehydrogenase inhibitors in SARS-CoV-2 infection. Eur. J. Clin. Invest. 50, e13366 https://doi.org/10.1111/eci.13366.

Dunn, M.C.C., Knight, D.A., Waldman, W.J., 2011. Inhibition of respiratory syncytial virus in vitro and in vivo by the immunosuppressive agent leflunomide. Antivir. Ther. 16, 309–317. https://doi.org/10.3851/IMP1763.

Fitzgerald, G.A., 1987. Dipyridamole. N. Engl. J. Med. 316, 1247–1257. https://doi.org/10.1056/NEJM198705143162005.

Garegnani, L., Styrmisdóttir, L., Roson Rodriguez, P., Escobar Liquitay, C.M., Esteban, I., Franco, J.V., 2021. Palivizumab for preventing severe respiratory syncytial virus (RSV) infection in children. Cochrane Database Syst. Rev. 11 https://doi.org/10.1002/14651858.CD013757.pub2. CD013757.

Grandin, C., Hourani, M.L., Janin, Y.L., Dauzonne, D., Munier-Lehmann, H., Paturet, A., Taborik, F., Vabret, A., Contamin, H., Tangy, F., Vidalain, P.O., 2016. Respiratory syncytial virus infection in macaques is not suppressed by intranasal sprays of pyrimidine biosynthesis inhibitors. Antivir. Res. 125, 58–62. https://doi.org/10.1016/j.antiviral.2015.11.006, 2016.

Gregov, D., Jenkins, A., Duncan, E., Sieber, D., Rodgers, S., Duncan, B., Bochner, F., Lloyd, J., 1987. Dipyridamole: pharmacokinetics and effects on aspects of platelet function in man. Br. J. Clin. Pharmacol. 24, 425–434. https://doi.org/10.1111/j.1365-2125.1987.tb03194.x.

Gribaudo, G., Riera, L., Rudge, T.L., Caposio, P., Johnson, L.F., Landolfo, S., 2002. Human cytomegalovirus infection induces cellular thymidylate synthase gene expression in quiescent fibroblasts. J. Gen. Virol. 83, 2983–2993. https://doi.org/10.1099/0022-1317-83-12-2983.

Gribaudo, G., Riera, L., Caposio, P., Maley, F., Landolfo, S., 2003. Human cytomegalovirus requires cellular deoxycytidylate deaminase for replication in quiescent cells. J. Gen. Virol. 84, 1437–1441. https://doi.org/10.1099/vir.0.18979-0.

Hammitt, L.L., Dagan, R., Yuan, Y., Baca Cots, M., Bosheva, M., Madhi, S.A., Muller, W. J., Zar, H.J., Brooks, D., Grenham, A., Wählby Hamrén, U., Mankad, V.S., Ren, P., Takas, T., Abram, M.E., Leach, A., Griffin, M.P., Villafana, T., MELODY Study Group, 2022. Nirsevimab for prevention of RSV in healthy late-preterm and term infants. N. Engl. J. Med. 386, 837–846. https://doi.org/10.1056/NEJMoa2110275.

Hansen, C.L., Chaves, S.S., Demont, C., Viboud, C., 2022. Mortality associated with influenza and respiratory syncytial virus in the US, 1999-2018. JAMA Netw. Open 5, e220527. https://doi.org/10.1001/jamanetworkopen.2022.0527.

Hasan, S., Sebo, P., Osicka, R., 2018. A guide to polarized airway epithelial models for studies of host-pathogen interactions. FEBS J. 285, 4343–4358. https://doi.org/10.1111/febs.14582.

Heylen, E., Neyts, J., Jochmans, D., 2017. Drug candidates and model systems in respiratory syncytial virus antiviral drug discovery. Biochem. Pharmacol. 127, 1–12. https://doi.org/10.1016/j.bcp.2016.09.014.

Jain, H., Schweitzer, J.W., Justice, N.A., 2022. Respiratory syncytial virus infection. In: StatPearls [Internet], Treasure Island (FL). StatPearls Publishing.

Jorquera, P.A., Anderson, L., Tripp, R.A., 2016. Human respiratory syncytial virus: an introduction. Methods Mol. Biol. 1442, 1–12. https://doi.org/10.1007/978-1-4939-3687-8_1.

Karimi, Z., Oskouie, A.A., Rezaei, F., Ajaminejad, F., Marashi, S.M., Azad, T.-M., 2022. The effect of influenza virus on the metabolism of peripheral blood mononuclear cells with a metabolomics approach. J. Med. Virol. 94, 4383–4392. https://doi.org/10.1002/jmv.27843.

Li, Y., Wang, X., Blau, D.M., Caballero, M.T., Feikin, D.R., Gill, C.J., Madhi, S.A., Omer, S. B., Simões, E.A.F., Campbell, H., Pariente, A.B., Bardach, D., Bassat, Q., Casalegno, J.-S., Chakhunashvili, G., Crawford, N., Danilenko, D., Do, L.A.H., Echavarria, M., Gentile, A., Gordon, A., Heikkinen, T., Huang, Q.S., Jullien, S., Krishnan, A., Lopez, E.L., Markić, J., Mira-Iglesias, A., Moore, H.C., Moyes, J., Mwananyanda, L., Nokes, D.J., Noordeen, F., Obodai, E., Palani, N., Romero, C., Salimi, V., Satav, A., Seo, E., Shchomak, Z., Singleton, R., Stolyarov, K., Stoszek, S.K., Von Gottberg, A., Wurzel, D., Yoshida, L.-M., Yung, C.F., Zar, H.J., Respiratory Virus Global Epidemiology Network, Nair, H., RESCEU Investigators, 2022. Global, regional, and national disease burden estimates of acute lower respiratory infections due to respiratory syncytial virus in children younger than 5 years in 2019: a systematic analysis. Lancet 399, 2047–2064. https://doi.org/10.1016/S0140-6736(22)00478-0.

Löffler, M., Carrey, E.A., Knecht, W., 2020. The pathway to pyrimidines: the essential focus on dihydroorotate dehydrogenase, the mitochondrial enzyme coupled to the respiratory chain. Nucleos Nucleot. Nucleic Acids 39, 1281–1305. https://doi.org/10.1080/15257770.2020.1723625.

Lucas-Hourani, M., Dauzonne, D., Jorda, P., Cousin, G., Lupan, A., Helynck, O., Caignard, G., Janvier, G., André-Leroux, G., Khiar, S., Escriou, N., Desprès, P., Jacob, Y., Munier-Lehmann, H., Tangy, F., Vidalain, P.-O., 2013. Inhibition of pyrimidine biosynthesis pathway suppresses viral growth through innate immunity. PLoS Pathog. 9, e1003678 https://doi.org/10.1371/journal.ppat.1003678.

Luganini, A., Caposio, P., Landolfo, S., Gribaudo, G., 2008. Phosphorothioate-modified oligodeoxynucleotides inhibit human cytomegalovirus replication by blocking virus entry. Antimicrob. Agents Chemother. 52, 1111–1120. https://doi.org/10.1128/AAC.00987-07.

Luganini, A., Sibille, G., Mognetti, B., Sainas, S., Pippione, A.C., Giorgis, M., Boschi, D., Lolli, M.L., Gribaudo, G., 2021. Effective deploying of a novel DHODH inhibitor against herpes simplex type 1 and type 2 replication. Antivir. Res. 189, 105057 https://doi.org/10.1016/j.antiviral.2021.105057.

Luthra, P., Naidoo, J., Pietzsch, C.A., De, S., Khadka, S., Anantpadma, M., Williams, C.G., Edwards, M.R., Davey, R.A., Bukreyev, A., Ready, J.M., Basler, C.F., 2018. Inhibiting pyrimidine biosynthesis impairs Ebola virus replication through depletion of nucleoside pools and activation of innate immune responses. Antivir. Res. 158, 288–302. https://doi.org/10.1016/j.antiviral.2018.08.012.

Madak, J.T., Cuthbertson, C.R., Chen, W., Showalter, H.D., Neamati, N., 2017. Design, synthesis, and characterization of brequinar conjugates as probes to study DHODH inhibition. Chemistry 23, 13875–13878. https://doi.org/10.1002/chem.201702999.

Martín-Vicente, M., González-Riaño, C., Barbas, C., Jiménez-Sousa, M.Á., Brochado-Kith, O., Resino, S., Martínez, I., 2020. Metabolic changes during respiratory syncytial virus infection of epithelial cells. PLoS One 15, e0230844. https://doi.org/10.1371/journal.pone.0230844.

McDonald, J.U., Kaforou, M., Clare, S., Hale, C., Ivanova, M., Huntley, D., Dorner, M., Wright, V.J., Levin, M., Martinon-Torres, F., Herberg, J.A., Tregoning, J.S., 2016. A simple screening approach to prioritize genes for functional analysis identifies a role for Interferon Regulatory Factor 7 in the control of respiratory syncytial virus disease. mSystems 1, e00051-16. https://doi.org/10.1128/mSystems.00051-16.

Munger, J., Bennett, B.D., Parikh, A., Feng, X.-J., McArdle, J., Rabitz, H.A., Shenk, T., Rabinowitz, J.D., 2008. Systems-level metabolic flux profiling identifies fatty acid synthesis as a target for antiviral therapy. Nat. Biotechnol. 26, 1179–1186. https://doi.org/10.1038/nbt.1500.

Nam, H.H., Ison, M.G., 2019. Respiratory syncytial virus infection in adults. BMJ 366, l5021. https://doi.org/10.1136/bmj.l5021.

Negishi, H., Taniguchi, T., Yanai, H., 2018. The interferon (IFN) class of cytokines and the IFN Regulatory Factor (IRF) transcription factor family. Cold Spring Harbor Perspect. Biol. 10, a028423. https://doi.org/10.1101/cshperspect.a028423.

Okesli, A., Khosla, C., Bassik, M.C., 2017. Human pyrimidine nucleotide biosynthesis as a target for antiviral chemotherapy. Curr. Opin. Biotechnol. 48, 127–134. https://doi.org/10.1016/j.copbio.2017.03.010.

Peters, G.J., 2018. Re-evaluation of Brequinar sodium, a dihydroorotate dehydrogenase inhibitor. Nucleos Nucleot. Nucleic Acids 37, 666–678. https://doi.org/10.1080/15257770.2018.1508692.

Pizzorno, G., Cao, D., Leffert, J.J., Russell, R.L., Zhang, D., Handschumacher, R.E., 2002. Homeostatic control of uridine and the role of uridine phosphorylase: a biological and clinical update. Biochim. Biophys. Acta 1587, 133–144. https://doi.org/10.1016/s0925-4439(02)00076-5.

Reis, R.A.G., Calil, F.A., Feliciano, P.R., Pinheiro, M.P., Nonato, M.C., 2017. The dihydroorotate dehydrogenases: past and present. Arch. Biochem. Biophys. 632, 175–191. https://doi.org/10.1016/j.abb.2017.06.019.

Sainas, S., Pippione, A.C., Lupino, E., Giorgis, M., Circosta, P., Gaidano, V., Goyal, P., Bonanni, D., Rolando, B., Cignetti, A., Ducime, A., Andersson, M., Järvå, M., Friemann, R., Piccinini, M., Ramondetti, C., Buccinnà, B., Al-Karadaghi, S., Boschi, D., Saglio, G., Lolli, M.L., 2018. Targeting myeloid differentiation using potent 2-hydroxypyrazolo[1,5- a]pyridine scaffold-based human dihydroorotate dehydrogenase inhibitors. J. Med. Chem. 61, 6034–6055. https://doi.org/10.1021/acs.jmedchem.8b00373.

Sainas, S., Giorgis, M., Circosta, P., Gaidano, V., Bonanni, D., Pippione, A.C., Bagnati, R., Passoni, A., Qiu, Y., Cojocaru, C.F., Canepa, B., Bona, A., Rolando, B., Mishina, M., Ramondetti, C., Buccinnà, B., Piccinini, M., Houshmand, M., Cignetti, A., Giraudo, E., Al-Karadaghi, S., Boschi, D., Saglio, G., Lolli, M.L., 2021. Targeting acute myelogenous leukemia using potent human dihydroorotate dehydrogenase inhibitors based on the 2-hydroxypyrazolo[1,5- *a*]pyridine scaffold: SAR of the biphenyl moiety. J. Med. Chem. 64, 5404–5428. https://doi.org/10.1021/acs.jmedchem.0c01549.

Sainas, S., Giorgis, M., Circosta, P., Poli, G., Alberti, M., Passoni, A., Gaidano, V., Pippione, A.C., Vitale, N., Bonanni, D., Rolando, B., Cignetti, A., Ramondetti, C., Lanno, A., Ferraris, D.M., Canepa, B., Buccinnà, B., Piccinini, M., Rizzi, M., Saglio, G., Al-Karadaghi, S., Boschi, D., Miggiano, R., Tuccinardi, T., Lolli, M.L., 2022. Targeting acute myelogenous leukemia using potent human dihydroorotate dehydrogenase inhibitors based on the 2-hydroxypyrazolo[1,5-a]pyridine scaffold: SAR of the aryloxyaryl moiety. J. Med. Chem. 65, 12701–12724. https://doi.org/10.1021/acs.jmedchem.2c00496.

Schaper, W., 2005. Dipyridamole, an underestimated vascular protective drug. Cardiovasc. Drugs Ther. 19, 357–363. https://doi.org/10.1007/s10557-005-4659-6.

Sepúlveda, C.S., García, C.C., Damonte, E.B., 2022. Inhibitors of nucleotide biosynthesis as candidates for a wide spectrum of antiviral chemotherapy. Microorganisms 10, 1631. https://doi.org/10.3390/microorganisms10081631.

Sibille, G., Luganini, A., Sainas, S., Boschi, D., Lolli, M.L., Gribaudo, G., 2022. The novel hDHODH inhibitor MEDS433 prevents Influenza virus replication by blocking pyrimidine biosynthesis. Viruses 14, 2281. https://doi.org/10.3390/v14102281.

Simões, E.A.F., Madhi, S.A., Muller, W.J., Atanasova, V., Bosheva, M., Cabañas, F., Baca Cots, M., Domachowske, J.B., Garcia-Garcia, M.L., Grantina, I., Nguyen, K.A., Zar, H. J., Berglind, A., Cummings, C., Griffin, M.P., Takas, T., Yuan, Y., Wählby Hamrén, U., Leach, A., Villafana, T., 2023. Efficacy of nirsevimab against respiratory syncytial virus lower respiratory tract infections in preterm and term infants, and pharmacokinetic extrapolation to infants with congenital heart disease and chronic lung disease: a pooled analysis of randomised controlled trials. Lancet Child Adolesc. Health 7, 180–189. https://doi.org/10.1016/S2352-4642(22)00321-2.

Smee, D.F., Hurst, B.L., Day, C.W., 2012. D282, a non-nucleoside inhibitor of influenza virus infection that interferes with de novo pyrimidine biosynthesis. Antivir. Chem. Chemother. 22, 263–272. https://doi.org/10.3851/IMP2105.

Smith, S.E., Busse, D.C., Binter, S., Weston, S., Diaz Soria, C., Laksono, B.M., Clare, S., Van Nieuwkoop, S., Van den Hoogen, B.G., Clement, M., Marsden, M., Humphreys, I. R., Marsh, M., de Swart, R.L., Wash, R.S., Tregoning, J.S., Kellam, P., 2019. Interferon-Induced Transmembrane Protein 1 restricts replication of viruses that enter cells via the plasma membrane. J. Virol. 93, e02003-e02018 https://doi.org/10.1128/JVI.02003-18.

Soni, A., Kabra, S.K., Lodha, R., 2023. Respiratory syncytial virus infection: an update. Indian J. Pediatr. https://doi.org/10.1007/s12098-023-04613-w.

Stegmann, K.M., Dickmanns, A., Heinen, N., Blaurock, C., Karrasch, T., Breithaupt, A., Klopfleisch, R., Uhlig, N., Eberlein, V., Issmail, L., Herrmann, S.T., Schreieck, A., Peelen, E., Kohlhof, H., Sadeghi, B., Riek, A., Speakman, J.R., Groß, U., Görlich, D., Vitt, D., Müller, T., Grunwald, T., Pfaender, S., Balkema-Buschmann, A., Dobbelstein, M., 2022. Inhibitors of dihydroorotate dehydrogenase cooperate with molnupiravir and N4-hydroxycytidine to suppress SARS-CoV-2 replication. iScience 25, 104293. https://doi.org/10.1016/j.isci.2022.104293.

Tejada, S., Martinez-Reviejo, R., Karakoc, H.N., Peña-López, Y., Manuel, O., Rello, J., 2022. Ribavirin for treatment of subjects with respiratory syncytial virus-related infection: a systematic review and meta-analysis. Adv. Ther. 39, 4037–4051. https://doi.org/10.1007/s12325-022-02256-5.

Wang, Q.-Y., Bushell, S., Qing, M., Xu, H.Y., Bonavia, A., Nunes, S., Zhou, J., Poh, M.K., Florez de Sessions, P., Niyomrattanakit, P., Dong, H., Hoffmaster, K., Goh, A., Nilar, S., Schul, W., Jones, S., Kramer, L., Compton, T., Shi, P.-Y., 2011. Inhibition of dengue virus through suppression of host pyrimidine biosynthesis. J. Virol. 85, 6548–6556. https://doi.org/10.1128/JVI.02510-10.

Ward, J.L., Sherali, A., Mo, Z.P., Tse, C.M., 2000. Kinetic and pharmacological properties of cloned human equilibrative nucleoside transporters, ENT1 and ENT2, stably expressed in nucleoside transporter-deficient PK15 cells. Ent2 exhibits a low affinity

for guanosine and cytidine but a high affinity for inosine. J. Biol. Chem. 275, 8375–8381. https://doi.org/10.1074/jbc.275.12.8375.

Yang, Y., Cao, L., Gao, H., Wu, Y., Wang, Y., Fang, F., Lan, T., Lou, Z., Rao, Y., 2019. Discovery, optimization, and target identification of novel potent broad-spectrum antiviral inhibitors. J. Med. Chem. 62, 4056–4073. https://doi.org/10.1021/acs.jmedchem.9b00091.

Zheng, Y., Li, S., Song, K., Ye, J., Li, W., Zhong, Y., Feng, Z., Liang, S., Cai, Z., Xu, K., 2022. A broad antiviral strategy: inhibitors of human DHODH pave the way for host-targeting antivirals against emerging and re-emerging viruses. Viruses 14, 928. https://doi.org/10.3390/v14050928.